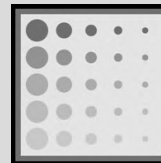


NERS/BIOE 481

Lecture 08 Radiation Detection

Michael Flynn, Adjunct Prof
Nuclear Engr & Rad. Science
mikef@umich.edu
mikef@rad.hfh.edu

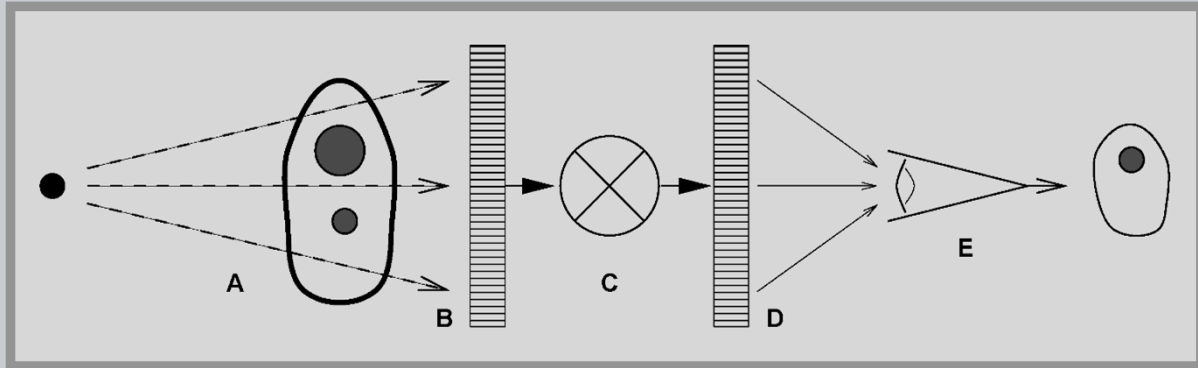


Henry Ford
Health System

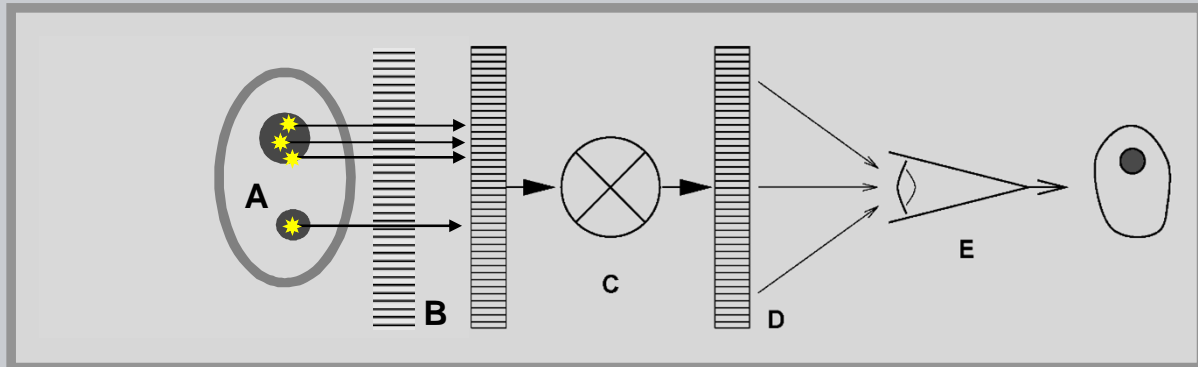
RADIOLOGY RESEARCH



Radiographic Imaging: Subject contrast (A) recorded by the detector (B) is transformed (C) to display values presented (D) for the human visual system (E) and interpretation.



Radioisotope Imaging: The detector records the radioactivity distribution by using a multi-hole collimator.





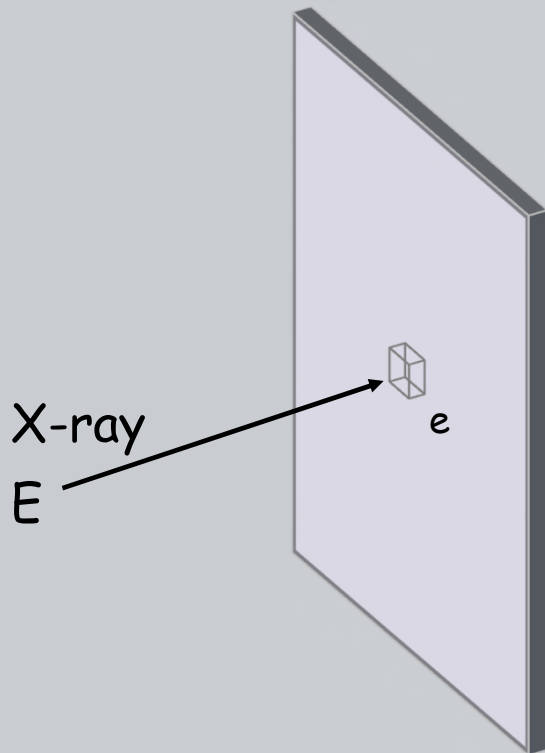
A. Conversion

1. Radiation Input

- a. X-ray absorption
- b. Energy deposition
- c. $p(e, E)de$



Desirable Detector Attributes for Radiation Imaging.

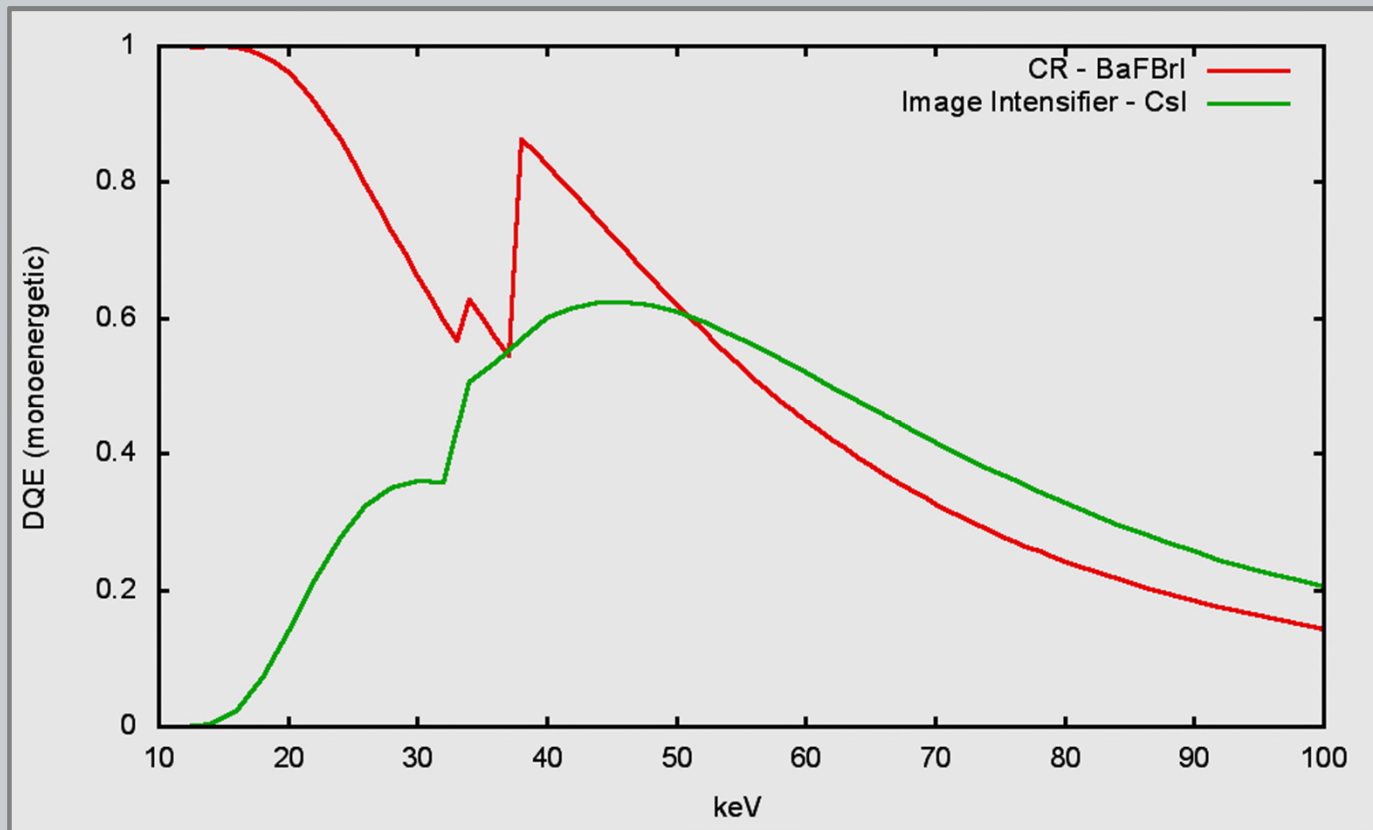


X-rays of energy E deposit energy e in a detector which is converted to charge n_e .

1. High Resolution:
 - Small detection elements
 - No signal blur
2. Large Signal:
 - High photon absorption
 - No energy loss
3. Low noise:
 - No quantum noise degradation
 - Negligible instrument noise



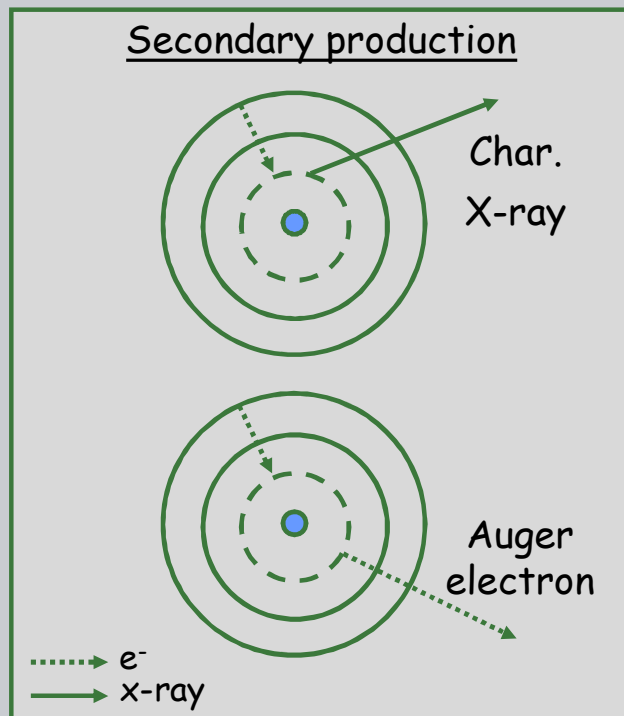
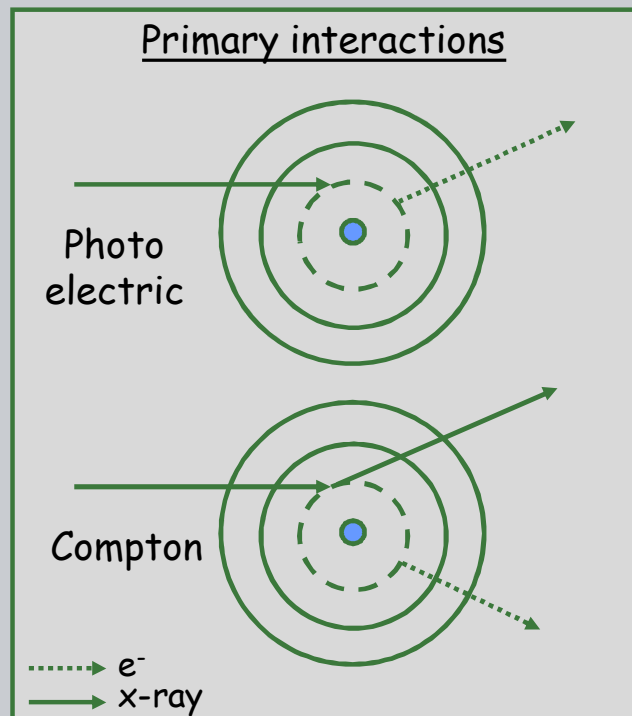
X-ray absorption in the detector varies significantly with the energy of the incident radiation



From XSPECT 3.6 detectors

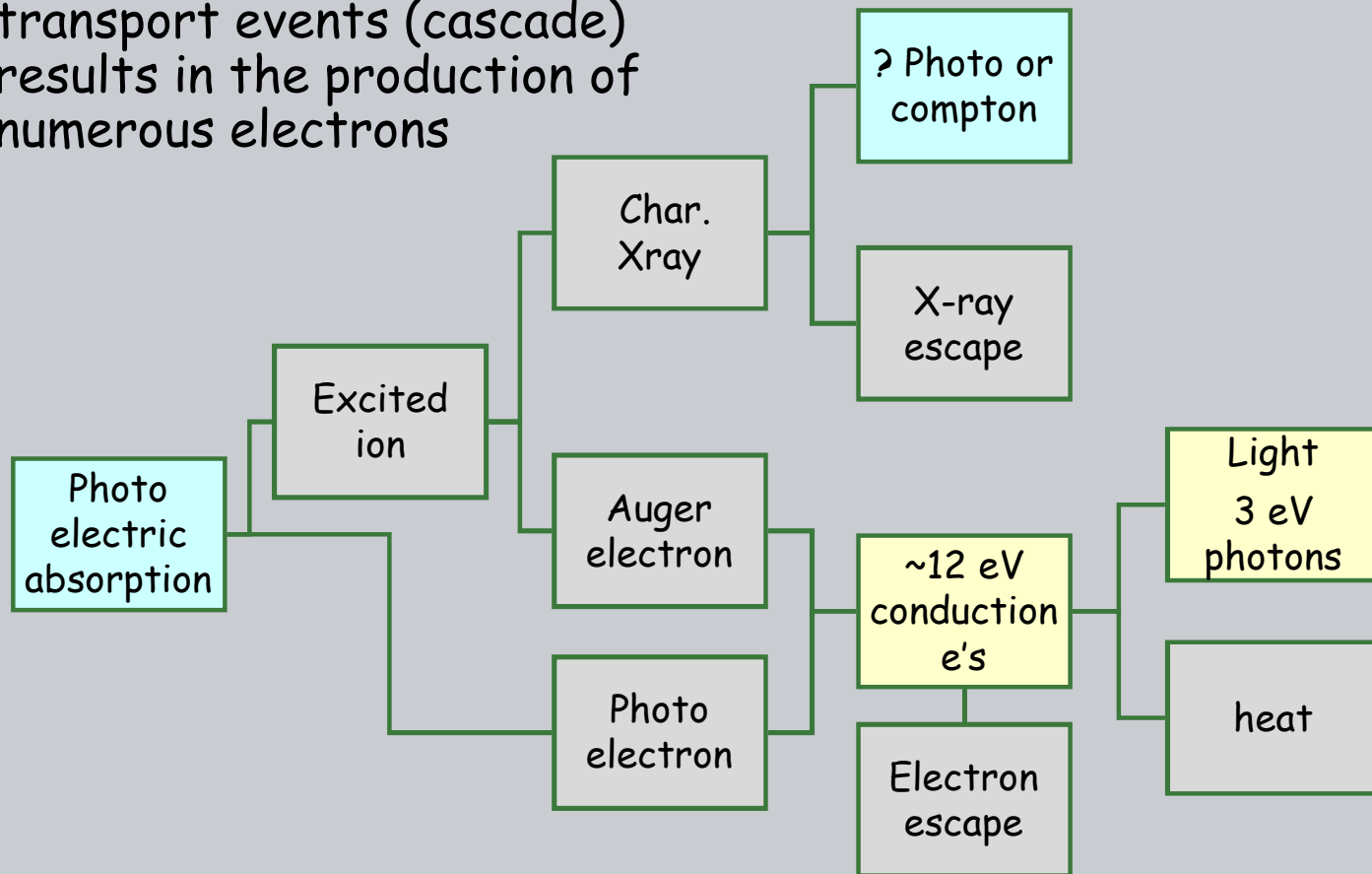


- X-ray interaction with either photoelectric or Compton interactions.
- Subsequent secondary radiation production effects the total energy deposition.





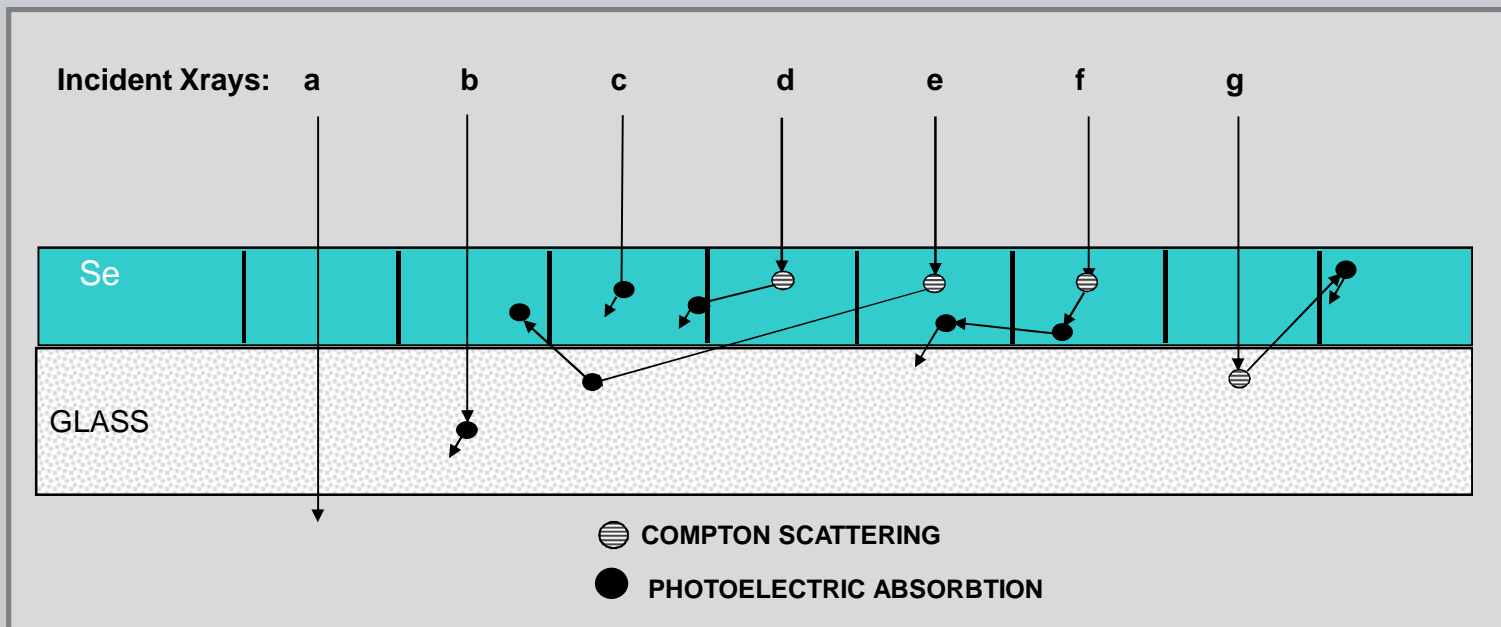
For each incident x-ray, a sequence of radiation transport events (cascade) results in the production of numerous electrons





V.A.1.b - energy deposition

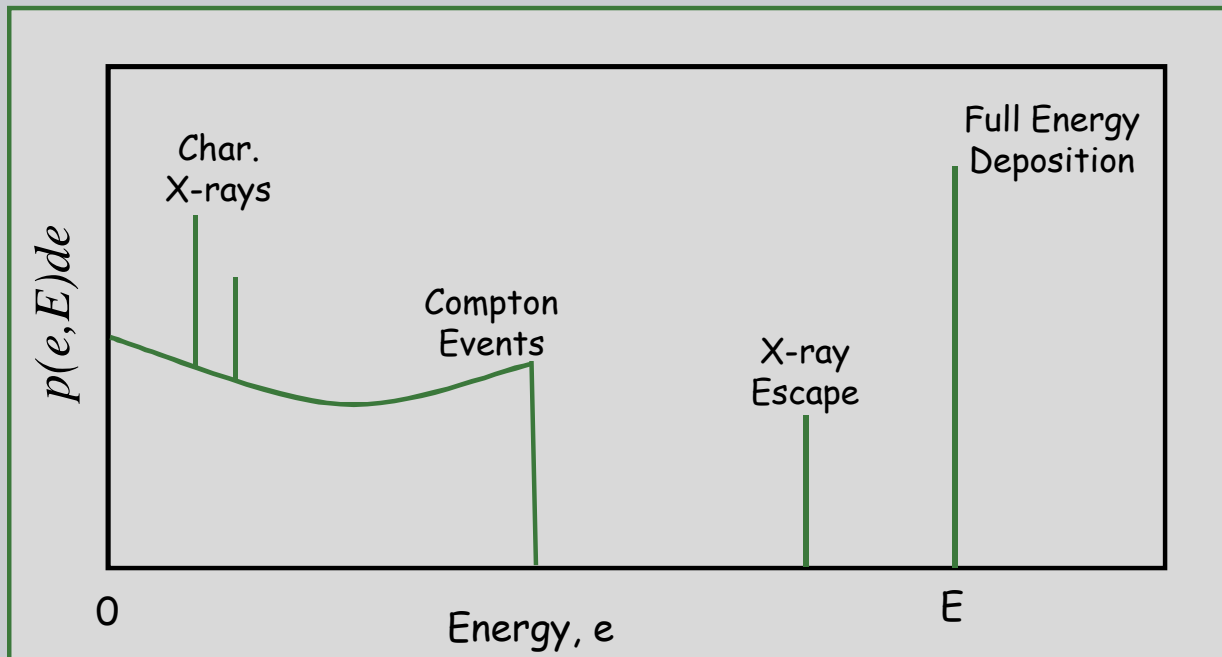
The energy deposited in the active region of a detection depends on the geometry and materials used to fabricate the detector assembly.





V.A.1.d - energy deposition probability

- For many x-rays incident on a detector, there will be a spectrum of deposited energy.
- The energy deposition probability is the deposition spectrum normalized to 1.0 (including the x-rays depositing 0 energy).





V.A.2 - Radiation Detector Output (7 charts)

A. Conversion

2. Detected Signal

a. Image values

b. Charge deposition probability

- For CR and DR systems, all radiation energy deposited in the detector, S_E , is converted to electrical charge, q_e , which is often collected on a capacitor.

S_E	signal, eV
S_v	signal, volts
q	charge, coulombs
q_e	charge in electrons
C	capacitance, farads

- CHARGE: $q_e = S_E / \varepsilon_e$, *electrons*

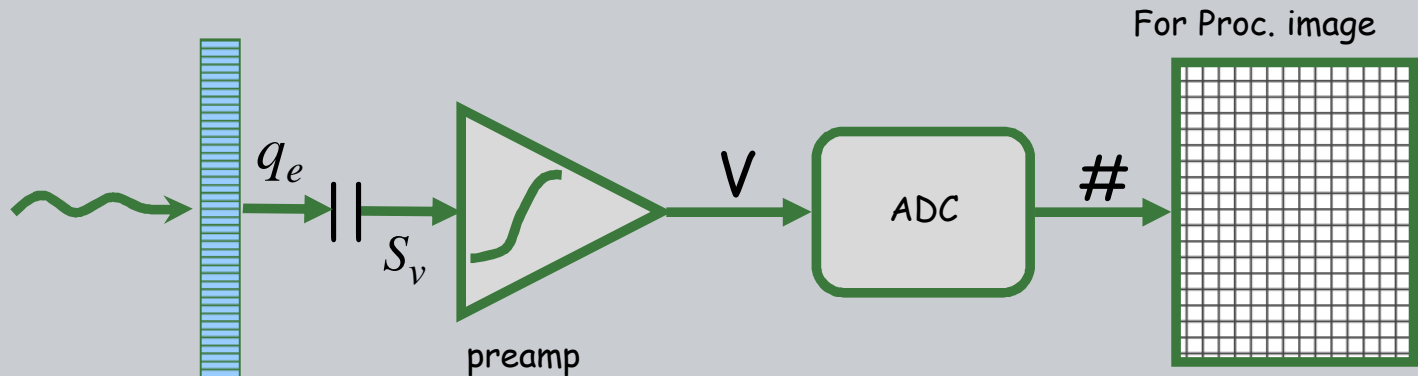
$$\varepsilon_e = eV / \textit{electron}$$

$$q = 1.602 \times 10^{-19} q_e \text{ , coulombs}$$

- VOLTAGE: $S_v = q / C$, *volts*

V.A.2.a - charge to image value conversion

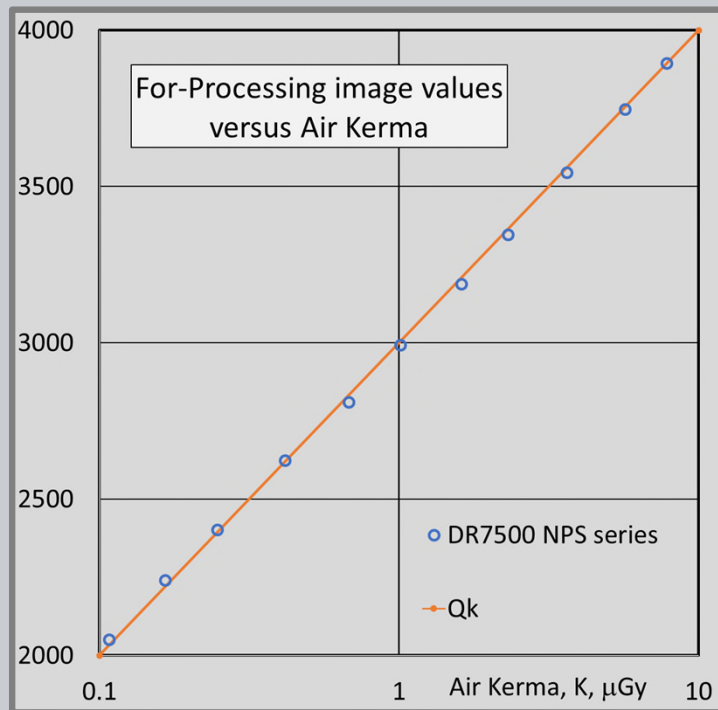
- Preamplifier circuits then amplify this voltage which is digitized using an analog to voltage converter (ADC) to produce 'For Processing' image values.
- Non-linear preamplifiers are often used so that the raw image values represent a wide range of exposures. Alternatively a non-linear input LUT can transform the ADC values.



'For Processing Image' is a DICOM standard term for images before image processing enhancements have been performed.

V.A.2.a - image value vs exposure

- Most For Processing image values are proportional to the log of the exposure incident on the detector.
- Small relative changes in exposure due to small tissue structures produce a fixed change in values regardless of the total tissue transmission.



Normalized For Processing Pixel Values (Q_K)

Q_K in relation radiation exposure input to the detector is defined as;

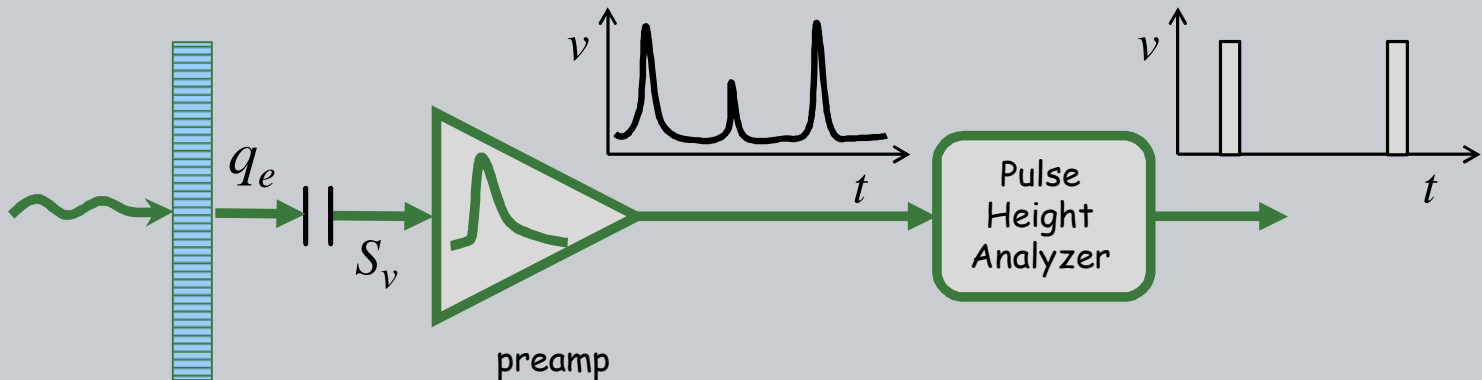
$$Q_K = 1000 \log_{10} [1000K]$$

Where K is the input air Kerma in μGy .

AAPM Report No. 116
Med.Phys. 36 (7) 2009

V.A.2.a - charge for each detection event.

- Radioisotope imaging systems collect the charge for each detection event which will be proportional to the deposited energy.
- Preamplifiers with fast time constants are used to obtain a pulse whose height is proportional to the collected charge.

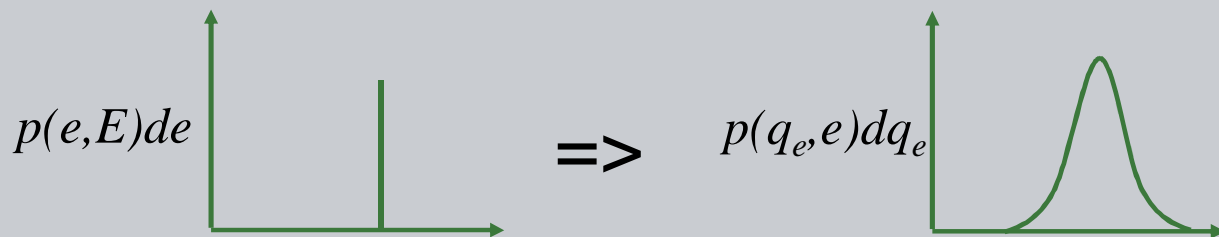


- We will examine how the position of the detected event is determined in L09.
- A new radiography system using pulse counting detectors will be covered in L10



V.A.2.b - charge variation

- The charge deposited in a detector may vary due to statistical fluctuations with the number of electrons produced, q_e , for a specific energy deposition E .



- The dispersion of q_e values resulting from energy deposition, e , is well described by Poisson statistics for the number of electrons.



V.A.2.b - charge deposition probability

- The overall probability for producing a charge q_e by radiation of energy E is the convolution of the energy deposition probability, $P(e, E)de$, and the charge dispersion probability, $P(q_e, e)dq_e$.

$$p(q_e, E)dE = \left[\int_0^E p(q_e, e)p(e, E)de \right] de$$

- For monoenergetic radiation of energy E_i , the charge signal from N_i detected photons is deduced from integration of the charge production probability.

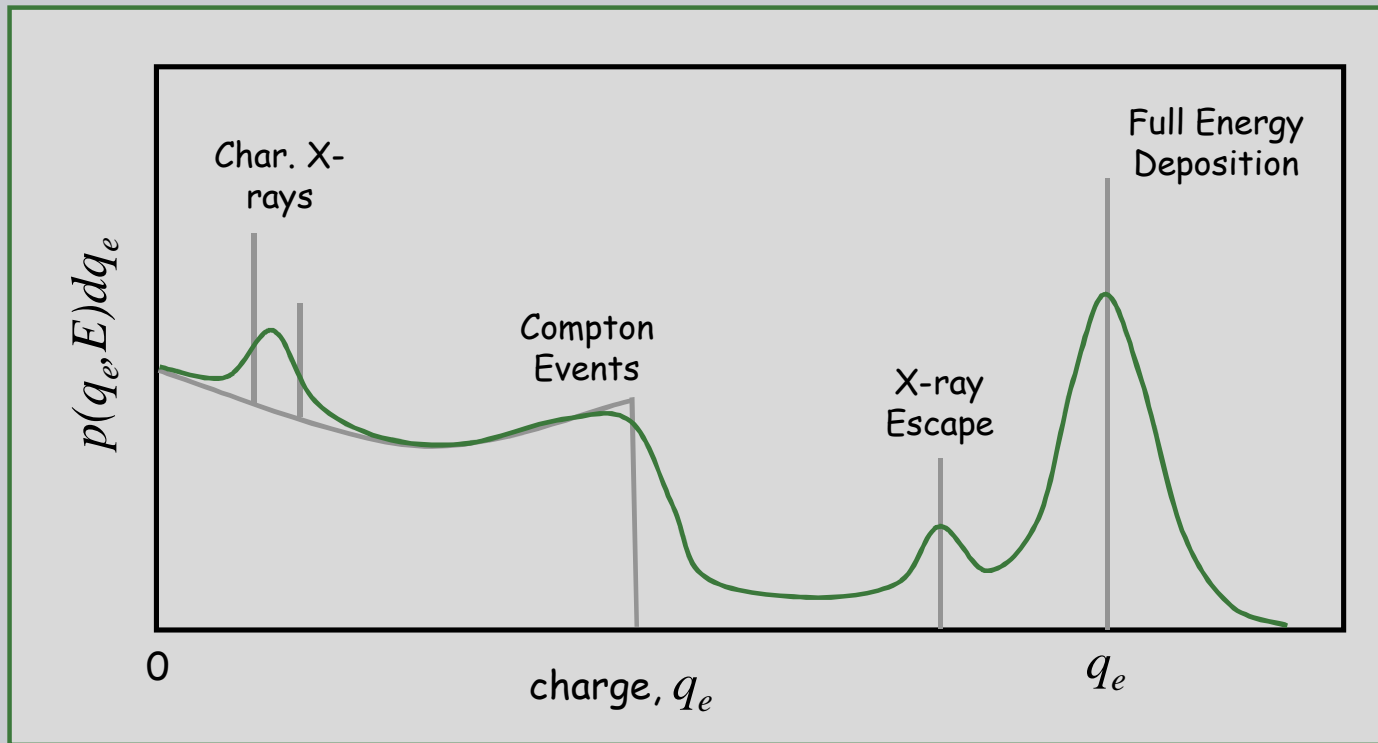
$$Q_e = N_i \int_0^{q_{\max}} q_e p(q_e, E_i) dq_e = N_i \bar{Q}_{E_i}$$

- This is equivalent to considering the average deposited charge from the discrete sum of all events.

$$Q_e = N_i \frac{\sum_{n=1}^{N_i} q_n}{N_i}$$



- Charge dispersion causes the recorded charge spectrum to be broadened relative to the deposited energy spectrum





A. Conversion

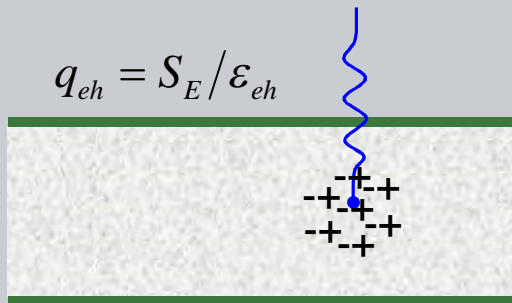
3. Direct Conversion

- a. charge production (eV per e-h pair)
- b. recombination (decay time)
- c. drift in an electric field (mobility)
- d. charge collection (μ - τ product)
- e. current leakage (resistivity)
- f. PbI_2 example

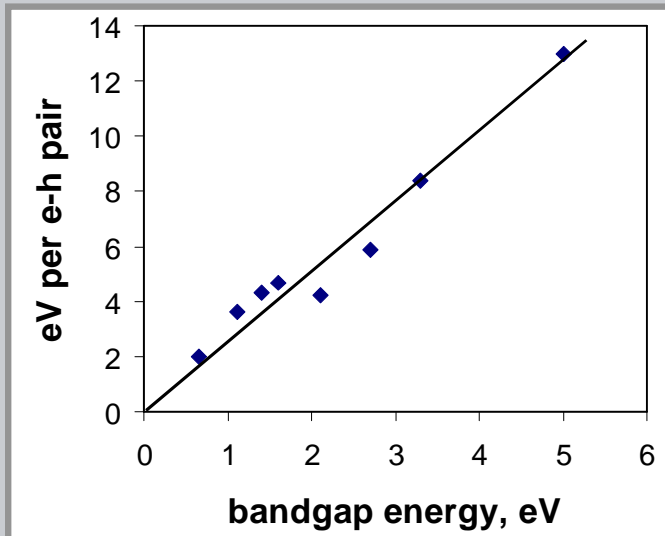
- For well structured semiconductor materials, the average energy required to create an electron-hole pair, is proportional to the bandgap energy.

$$\epsilon_{eh} , \text{ eV/ion-pair}$$

- Low bandgap materials provide good energy resolution for radiation detectors.



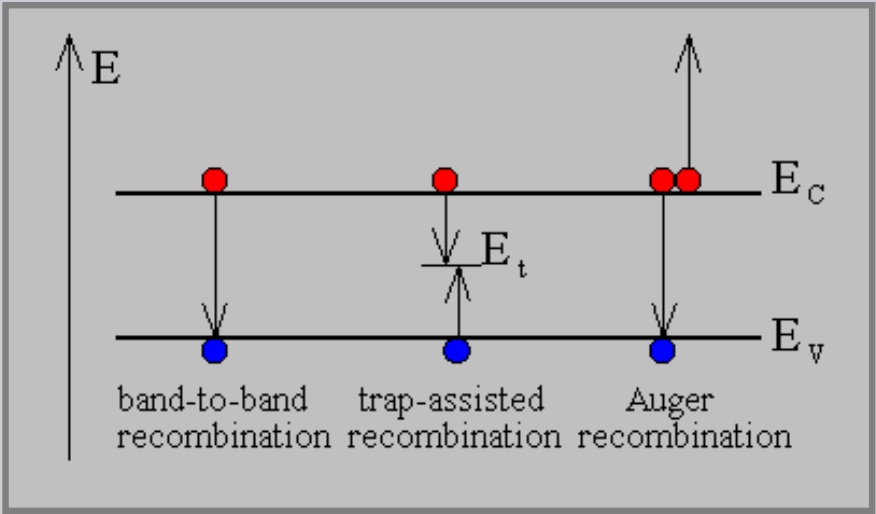
$$q_{eh} = S_E / \epsilon_{eh}$$



	<u>Z</u>	<u>gap eV</u>	<u>eV/e-h</u>
Diamond	6	5	13
SiC	6,10	3.3	8.4
Si	14	1.12	3.6
Ge	32	0.66	2
GaAs	31,33	1.4	4.3
CdZnTe	48,52	1.6	4.7
HgI ₂	80,53	2.1	4.2
TlBr	81,35	2.7	5.9



- Recombination of electrons and holes is a process by which both carriers annihilate each other. The electrons fall in one or multiple steps into the empty state which is associated with the hole.



<http://ece-www.colorado.edu/~bart/book/recomb.htm>

Recombination time - τ

If no further e-h pairs are formed, the population of e-h carriers will decay. The time constant of decay is the 'recombination time' or 'carrier lifetime'

<u>μsec</u>	τ_e	τ_h
Si	$>10^3$	$>10^3$
Ge	$>10^3$	2×10^3
CdTe	3	2

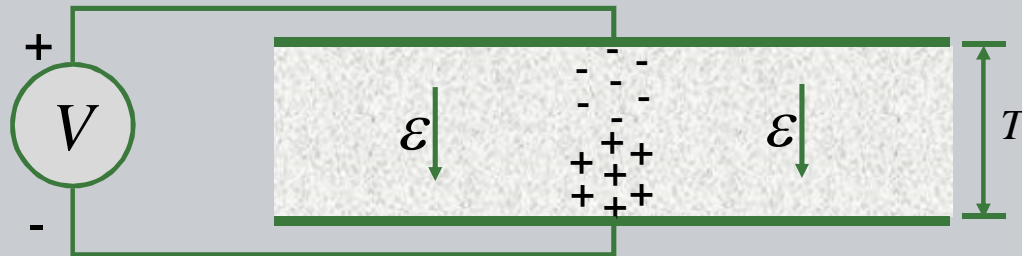
Owens, NIM, 2004



V.A.3.c -drift velocity (mobility).

For certain semi-conductive materials, electrons and holes will drift under the influence of an electric field until they either recombine to form a neutral atom or are electronically collected at a boundary.

$$\mathcal{E} = \frac{V}{T}$$



- Electron and ions drift in opposite direction from the ionized region near the point of x-ray interaction.
- The drift velocity is the product of the mobility and the electric field.

$$v_e = \mu_e \mathcal{E}$$

v_e : average drift velocity, cm/sec

μ_e : mobility, cm²/V-sec

cm²/V-sec

	μ_e	μ_h
Si	1400	1900
Ge	3900	1900
CdTe	1100	100

Owens, NIM, 2004



- The mean distance traveled in the recombination time, d_r , is the product of the drift velocity and the recombination time. This is equal to the product of the electric field, \mathcal{E} , and the 'mu-tau' product, i.e.

Owens, NIM, 2004

μ_e or μ_h (electron/hole mobility)
times τ (recombination time).

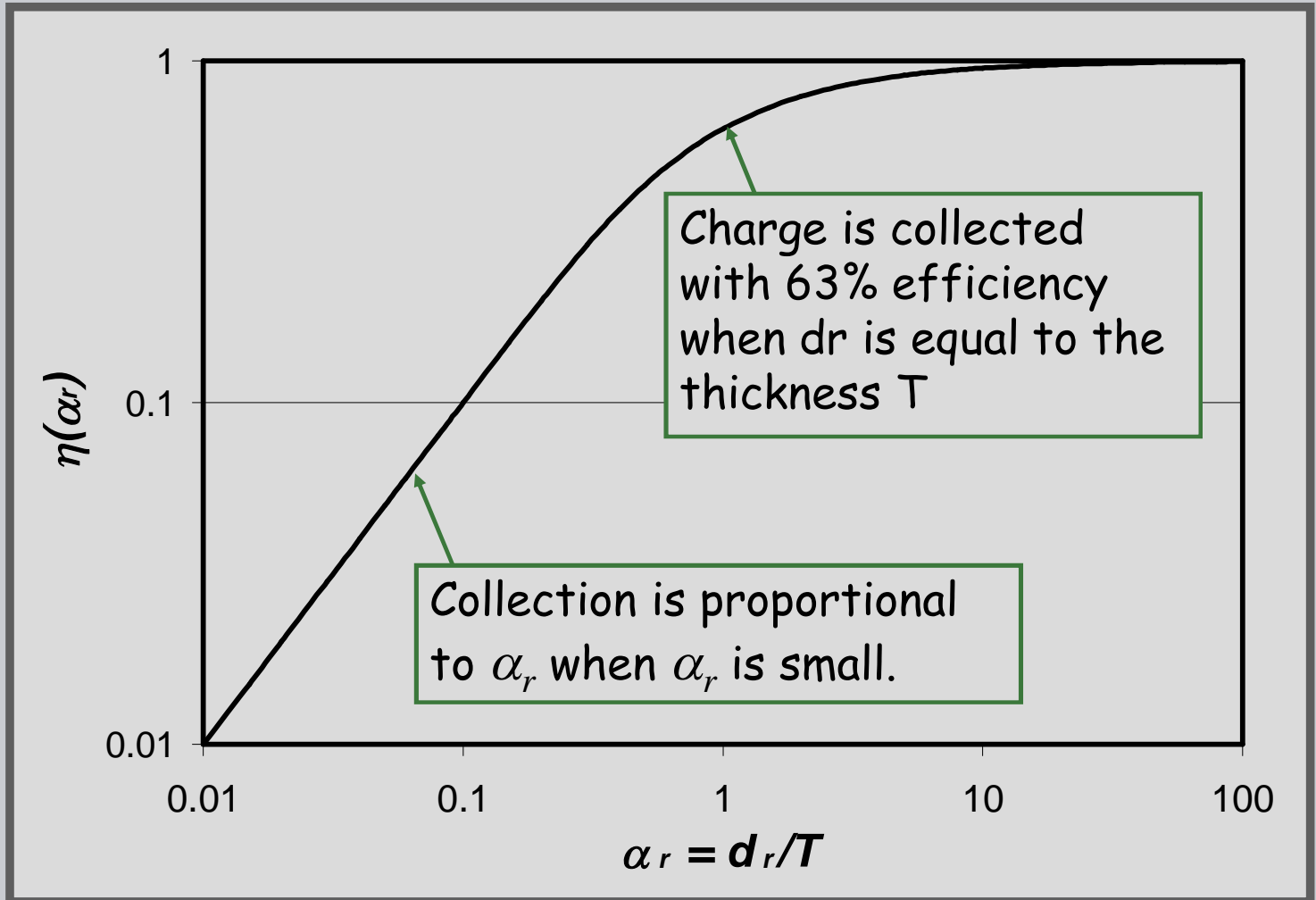
$$d_r = v_e \tau = \mu_e \tau \mathcal{E}$$

$\frac{\text{cm}^2/\text{V}}$	$\underline{\mu_e \tau}$	$\underline{\mu_h \tau}$
Si	>1	1
Ge	>1	>1
CdTe	3×10^{-3}	2×10^{-4}

- The efficiency for collecting charge, η_e , is related to the ratio of d_r and the detector thickness, T .

$$\alpha_r = d_r / T = \mu_e \tau \mathcal{E} / T = \mu_e \tau \frac{V}{T^2}$$

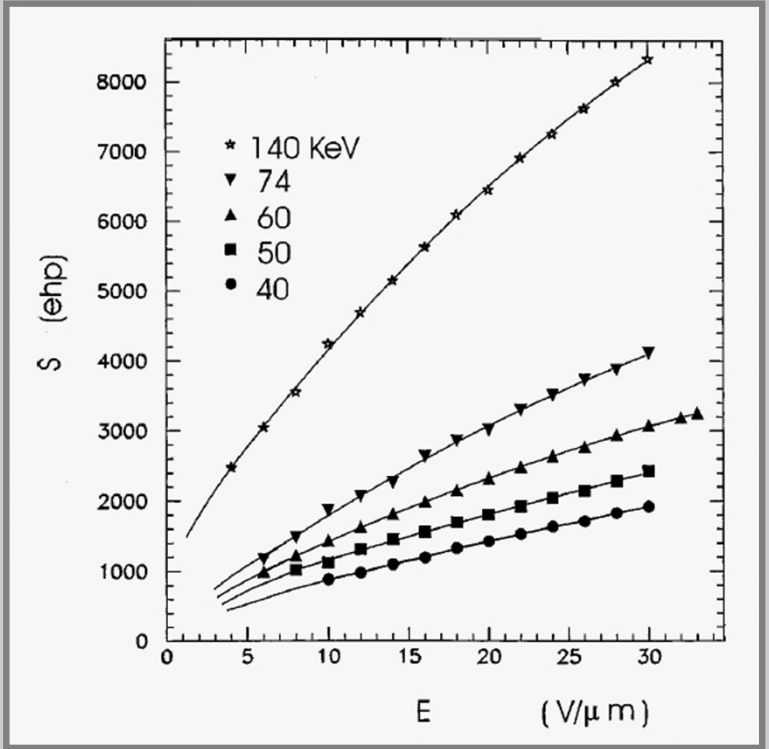
$$\eta_e = \alpha_r \left(1 - e^{-1/\alpha_r} \right) \quad \underline{\text{Hecht Formula}}$$



- The signal in electrons for amorphous selenium was reported by Blevis as a function of xray energy and electric field.
- The results are consistent with the Hecht equation for a collection efficiency of 0.1 and:

$$\mu_e \tau = 1.5E-08$$

$$\epsilon_{eh} = 5 \text{ eV}$$

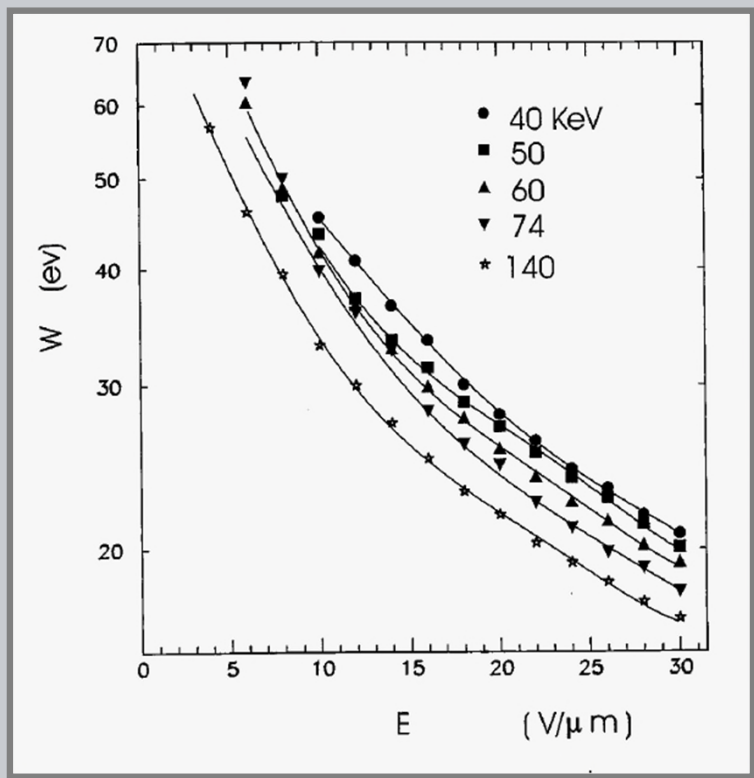


Blevis, J. Appl. Phys. 1999
0.15 mm a-Se film

Note: Bhatnagar reported the band gap energy for a-Se as about 2 eV (J. Appl. Phys, 1985).

- The eV deposited per collected electron, W , is used to predict the signal from an x-ray detector.
- When the Blevis data for selenium is plotted as W vs the electric field, a dependance on x-ray energy is seen.
- This is not consistent with the Hecht equation and suggests a charge density dependence for recombination.

Hijazi, J Mater Sci, 2018



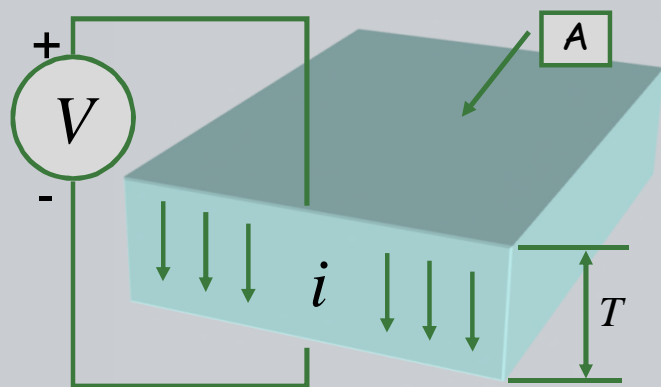
Blevis, J. Appl. Phys. 1999
0.15 mm a-Se film

Amorphous selenium direct conversion detectors have been used for radiography and mammography.



V.A.3.e -leakage current

- A small leakage current exists due to the voltage used to collect charge from each detector element.
- The element resistance is determined by the material resistivity, the element area, and the thickness.



ρ = material resistivity, $\Omega\text{-cm}$

$R = \rho (T/A)$, cell resistance, Ω

$i = V/R$, leakage current, amps

$i/A = V / \rho T$, amps/ mm^2



- The leakage current contributes to the signal in relation to the signal integration time, t_{int} .

$$Q_l = i_l t_{int}$$

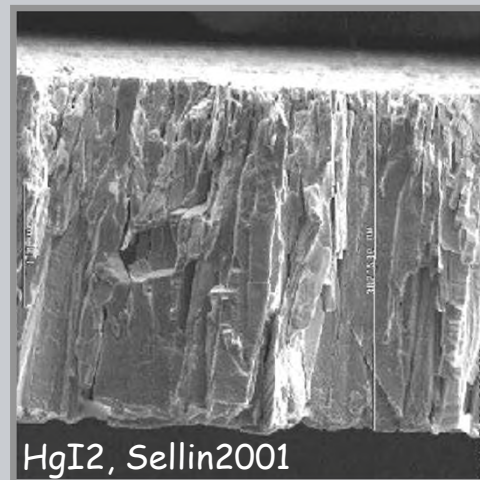
- While the signal can be corrected to eliminate the leakage current contribution, there remains an added noise from the number of electrons associated with the collected leakage current.

$$n_{le} = Q_l / 1.602E-19$$

$$\sigma_{le} = (Q_l / 1.602E-19)^{1/2}$$

V.A.3.f -HgI₂ and PbI₂ detector materials

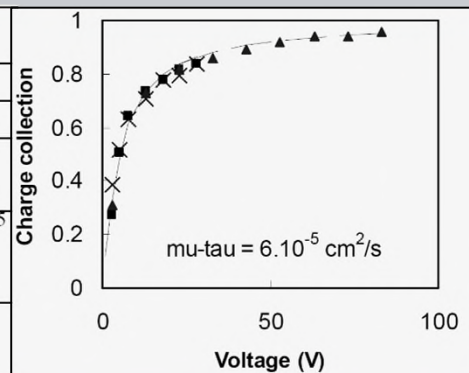
Polycrystalline mercuric iodide, HgI₂, and lead iodide, PbI₂, have been investigated as large area semi-conductor materials with high x-ray absorption.



Zentai et. al. SPIE MI 2003

- Relative to a-Se, improved absorption (high Z) and reduced Weff.
- Charge collection consistent with Hecht relation.

	Poly-HgI ₂	Poly-PbI ₂	a-Se
Atomic Number (Z)	80, 53	82, 53	34
Energy Band Gap (E _g) eV	2.1	2.3	2.2
Effective Charge Pair Formation Energy (W), eV	~5	~5.5	~42
Mobility Life-time Product ($\mu\tau$) cm ² /V	1.5x10 ⁻⁵	(hole) 1.8x10 ⁻⁶ (electron) 7x10 ⁻⁸	10 ⁻⁶ – 10 ⁻⁵
Operational Electric Field (E) V/micron	0.2-1	0.2-1	10





Consider a hypothetical PbI₂ detector operating as an Integrating Detector

Hypothetical Detector

$$\rho = 0.2E12 \Omega\text{-cm}$$

$$T = .010 \text{ cm (100 } \mu\text{m)}$$

$$A = (.010 \times .010) \text{ cm}^2$$

$$V = 50 \text{ Volts}$$

$$\mu\tau = 2E-6 \text{ cm}^2/\text{V}$$

$$t_{exp} = 1.00 \text{ secs}$$

As an integrating detector, the leakage current noise is small for exposures of 10,000 x-ray per detector element

X-ray Signal Noise

For the total absorption of a 20,000 eV x-ray,

- 4000 e's are produced (5 eV/ehp).
- ~2500 e's are collected (63%, Hecht eq., $dr = 1$)

For the detection of 10,000 x-rays (20 keV),

- 2.5 E+07 e's are collected (10,000 × 2500)
- Signal Noise: $2500(10,000)^{1/2} = 2.5 \text{ E}+05 \text{ e's}$.

This 1% noise is the x-ray quantum signal noise (mottle) associated with 10,000 detected x-rays.

Leakage Noise

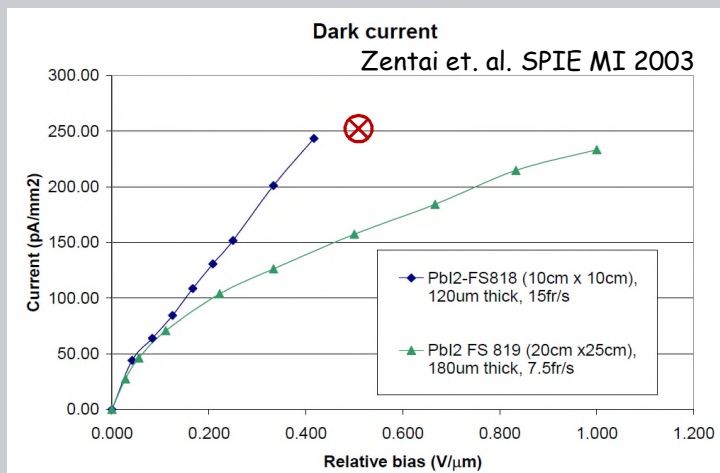
Charge collected during a 1.0 S integration time;

- Leakage Current = 2.5E-12 amps (250 pA/mm²).
- 15.61E+06 e's are collected in $t_{exp} = 1.0 \text{ S}$.
- Leakage noise: $(32.96E+06)^{1/2} = 3950 \text{ e's}$.
- This leakage noise is .016 times the quantum noise.



V.A.3.f -PbI₂ example

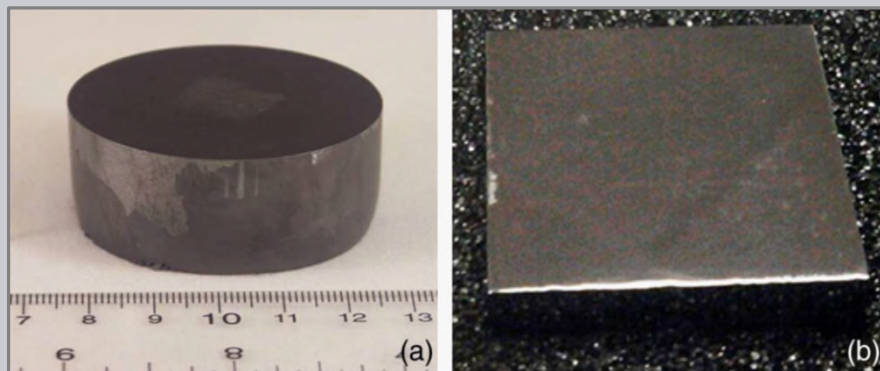
The resistivity and resultant leakage current for the 'hypothetical detector' is consistent with the dark current of a prototype device.



- While prototype radiography detectors were developed in the early 2000s, commercialization has not been successful.
- a-Se continues to be commercially successful due in part to material fabrication.



- The heterogeneous material structure of PbI_2 prohibits consistent measures of the charge from each x-ray.
- The lower resistivity of CZT prohibits its use as an integrating x-ray detector. However, the crystalline nature of CZT makes it attractive for photon counting detectors and radioisotope imaging cameras.



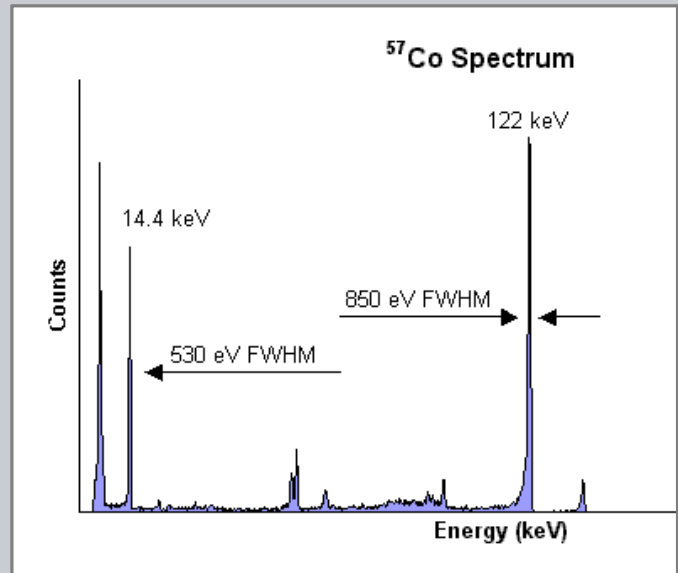
(a) Grown CZT ingot, (b) cut polished CZT detector.
Chaudhuri, IEEE TNS, VOL. 61, NO. 2, April 2014



Material	CZT	CdTe	HgI2	PbI2	α -Se
Atomic Nos.	48,30,52	48,52	80,52	82,52	34
Resistivity	3×10^{10}	10^9	10^{13}	10^{12}	10^{12}
mu-tau (e)	6×10^{-3}	3×10^{-3}	1×10^{-4}	8×10^3	5×10^9

Higher mu-tau product provides good charge collection and consistent measurement of energy.

In the coming lectures we will learn of CdTe/CZT detectors used for radioisotope imaging and photon counting radiography/CT systems.

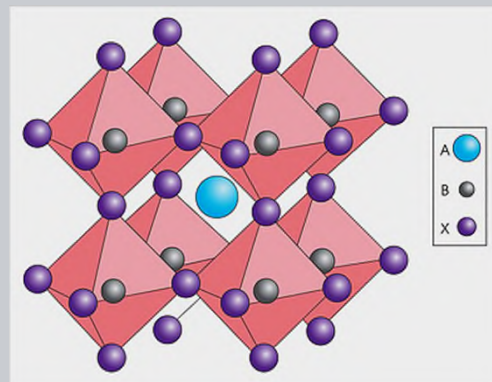


Signal spectrum from monoenergetic 122 keV photons using a CdTe detector. Amptek, Inc.



Perovskite crystals have been of recent interest for x-ray imaging:

- High μ - τ product
- Good x-ray absorption (high Z)



Sensitive X-ray detectors made of methylammonium lead tribromide perovskite single crystals

Wei H, Fang Y, Mulligan P et.al.; nature photonics, 21 MARCH 2016 (online).

“The large mobilities and carrier lifetimes of hybrid perovskite single crystals and the high atomic numbers of Pb, I and Br make them ideal for X-ray and gamma-ray detection. Here, we report a sensitive X-ray detector made of methylammonium lead bromide perovskite single crystals. A record-high mobility–lifetime product of $1.2 \times 10^{-2} \text{ cm}^2 \text{ V}^{-1}$ and an extremely small surface charge recombination velocity of 64 cm s^{-1} are realized by reducing the bulk defects and passivating surface traps...”

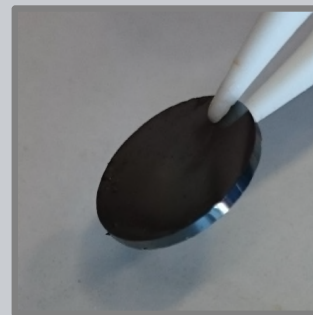
Jinsong Huang Group at UNC

<http://huangjinsong.wixsite.com/group>

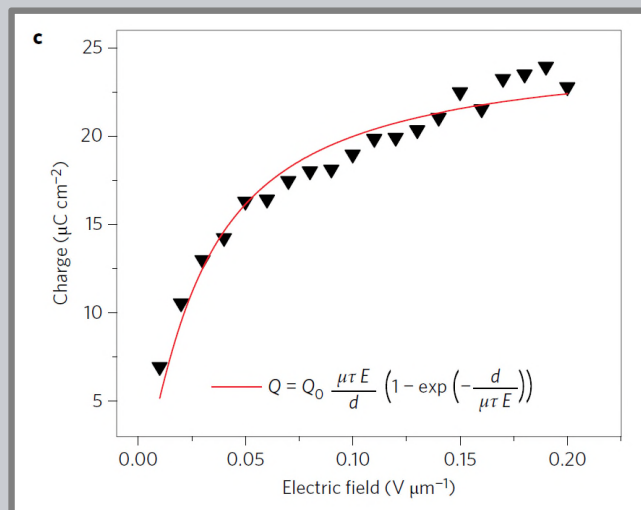
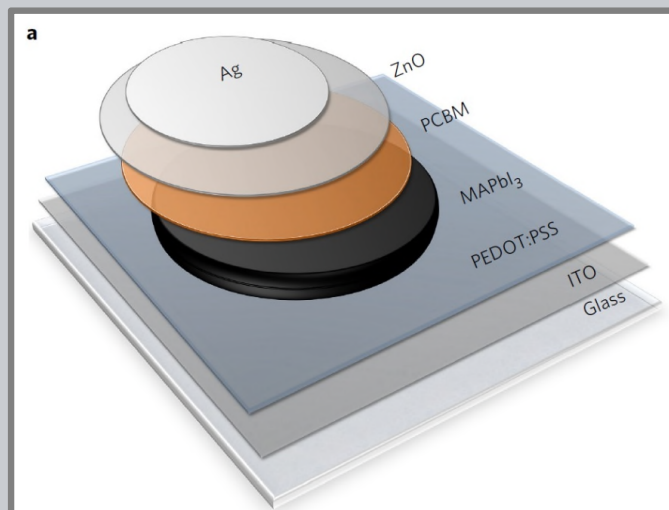


V.A.3.f - MAPbI₃

- High-performance direct conversion X-ray detectors based on sintered hybrid lead triiodide perovskite wafers
- Shrestha, Nature Photonics, June 2017



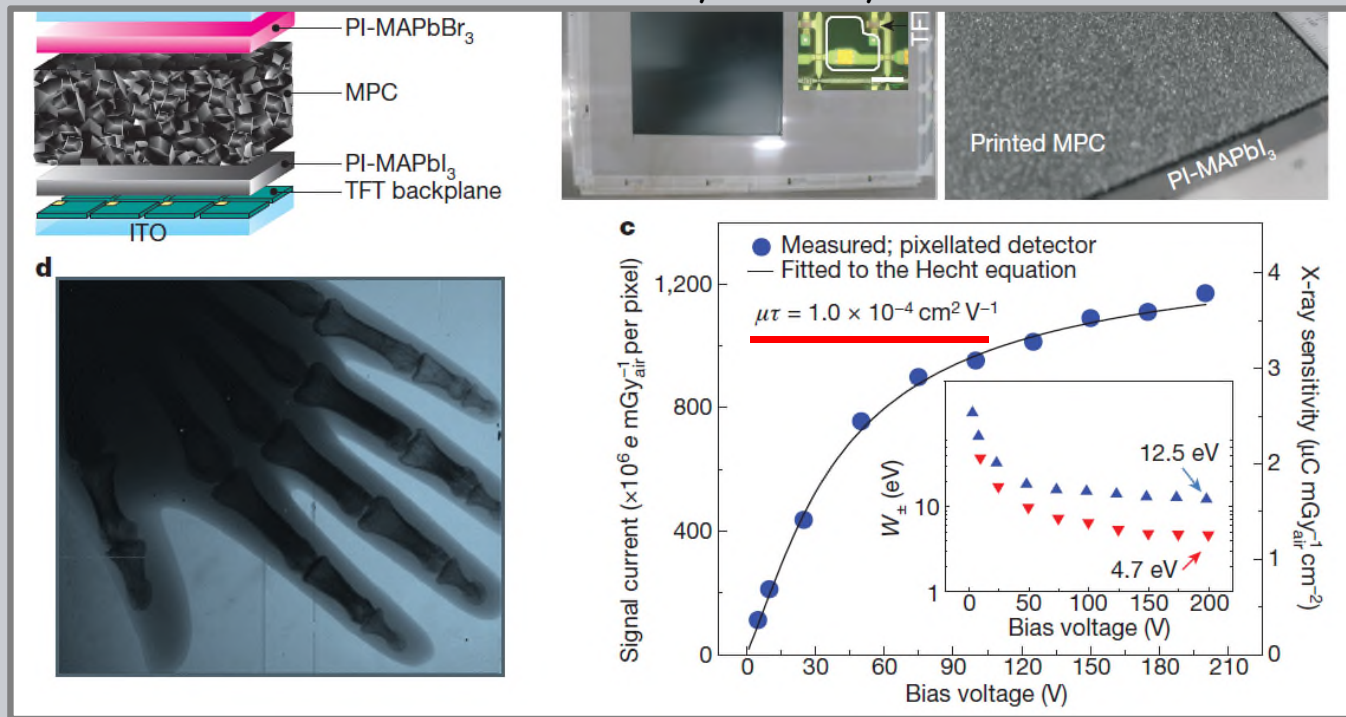
“we present a sintering process to ... thick MAPbI₃ wafers. The wafer conserves the structural and optical properties of the microcrystalline starting material. Ambipolar charge transport is demonstrated with a mobility of 0.45–0.7 cm² V⁻¹ s⁻¹. Under X-ray exposure, a $\mu\tau$ product of $\sim 2 \times 10^{-4}$ cm² V⁻¹ is measured”





Printable organometallic perovskite enables large-area, low-dose X-ray imaging

Kim, Nature, Oct 2017



“We report here an all-solution based (in contrast to conventional vacuum processing) synthetic route to producing printable polycrystalline perovskites with sharply faceted large grains having morphologies and optoelectronic properties comparable to those of single crystals.”

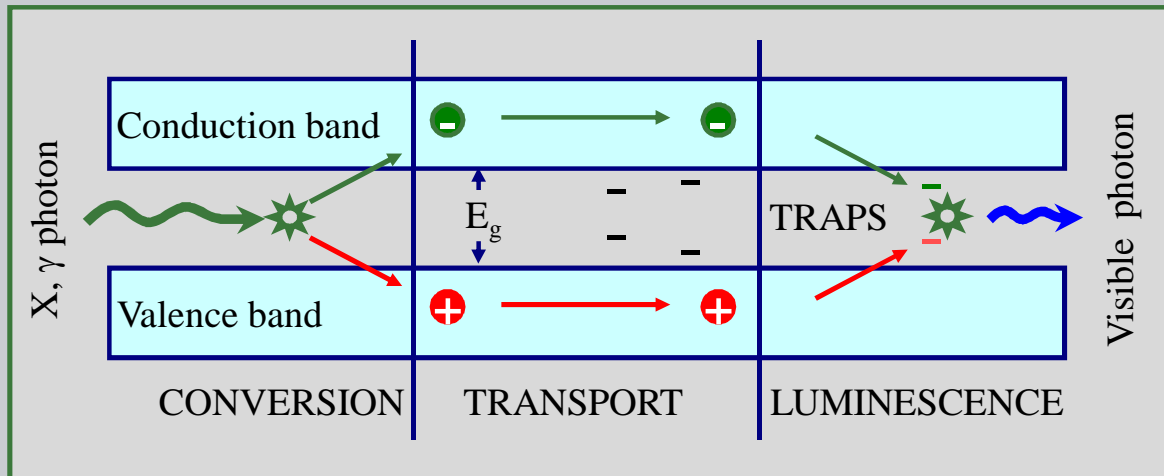


A. Conversion

4. Indirect Conversion

- a. The scintillation process
- b. Inorganic scintillator materials
- c. Photodetection
- d. Indirection conversion efficiency
- e. Signal deposition probability (spectra)

- A number of inorganic (usually crystal) materials have significant fluorescence yields when activated by ionizing radiation.
- The deposition of energy creates electron-hole pairs which emit low energy photons when they recombine.
- The fluorescence (scintillation) photons are in the visible to UV range and can be detected with light devices such as photomultiplier tubes, image intensifiers, or photodiodes.

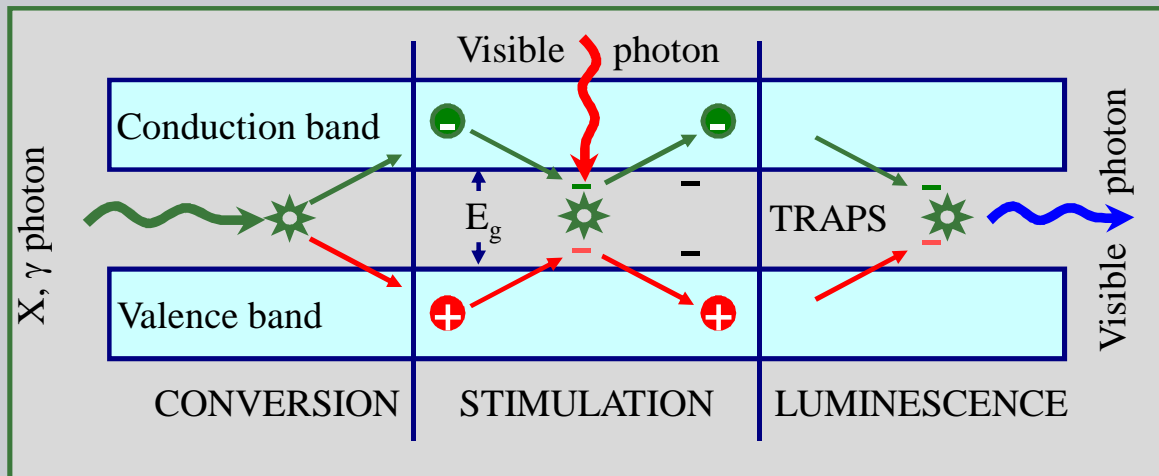


From: Nikl 2006, pg 38



V.A.4.a - Scintillation, storage phosphors

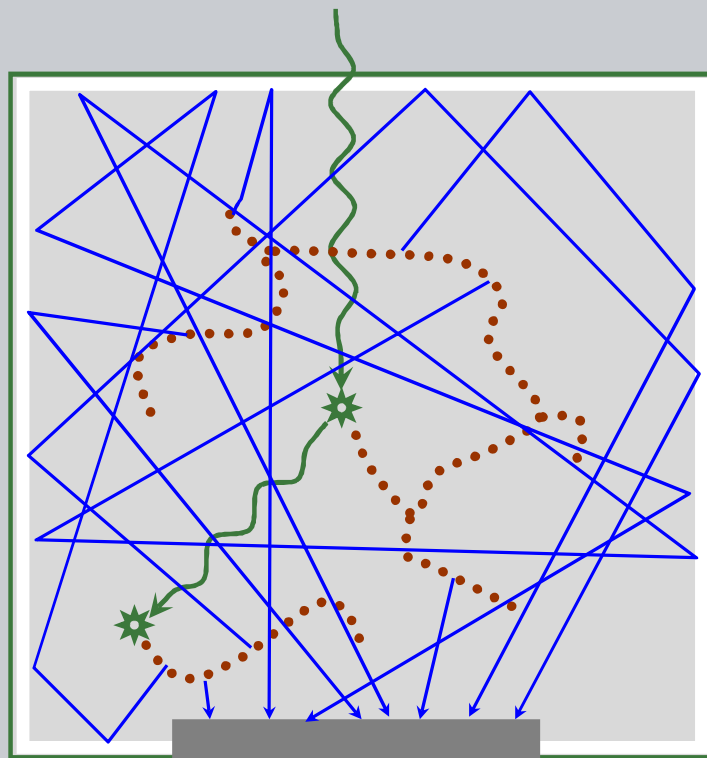
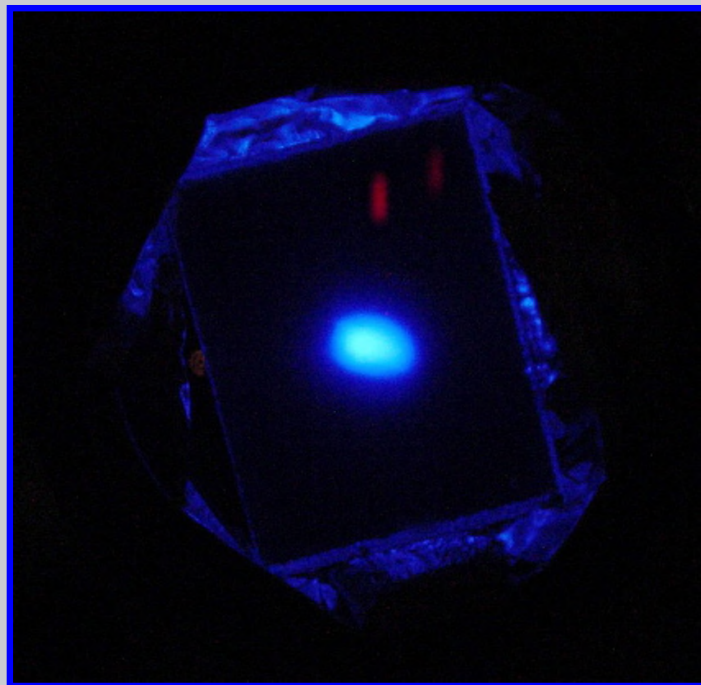
- For most scintillator materials, light photons are emitted with minimal time delay (prompt emission).
- For a few materials, the hole pairs produced are stored in trapped states until an excitation photon causes luminescent recombination (stimulated emission). These are called storage phosphors.





V.A.4.a - Scintillation cascade process

The absorption of a single X or gamma ray in a scintillator results in a radiation transport cascade producing many light photons (see slide # 7).



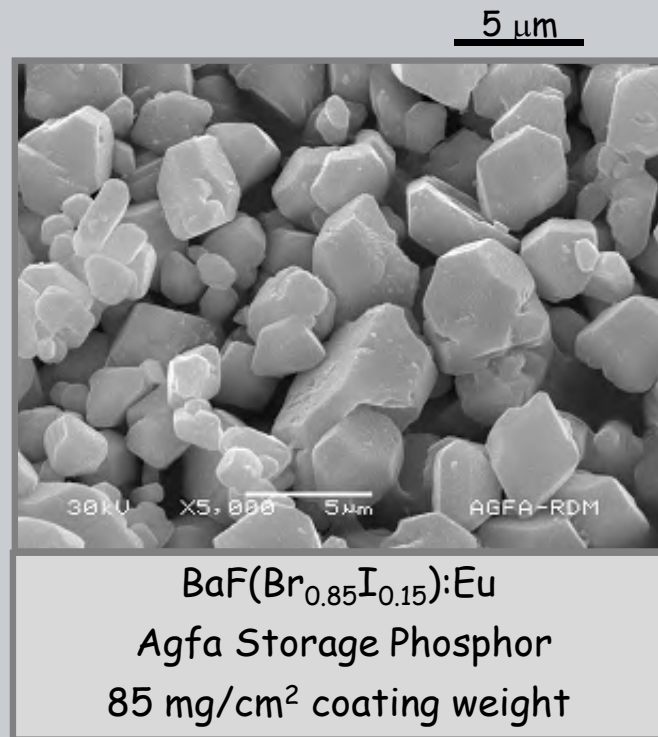
 X, γ ray

 electron

 Light photon

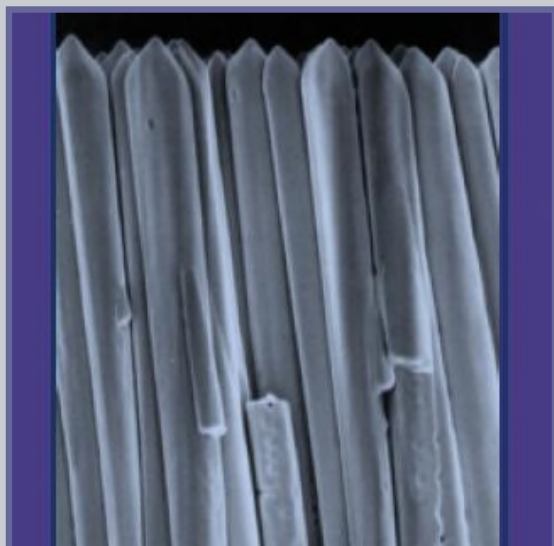
Granular Phosphors

- Traditional x-ray screens have been made from granular phosphor material. The screens are made on a stiff backing by sedimentation with a binder and coated with a protective layer.
- Grain sizes are typically between 2 and 10 microns.
- The screen thickness is usually reported as a coating weight which varies from 50 to 140 mg/cm².



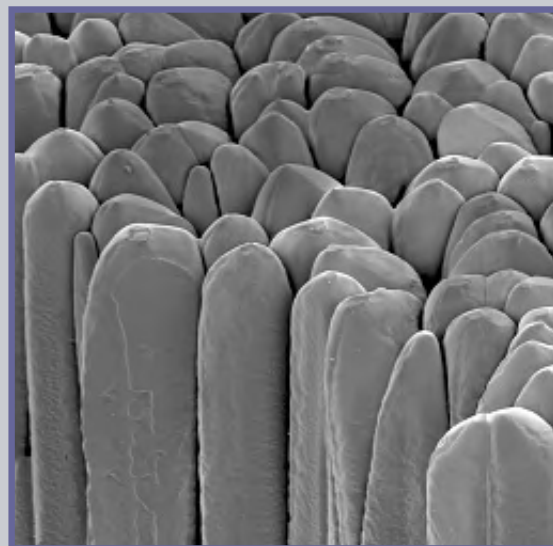
Needle Phosphors

- Phosphors grown as long thin rods emerging perpendicular to the screen surface are now used to achieve increased coating weight while still controlling the lateral spread of scintillation light.
- Coating weights of ~ 200 mg/cm² are typical (~ 500 microns).



CsI:Tl

Hamamatsu Prompt Phosphor

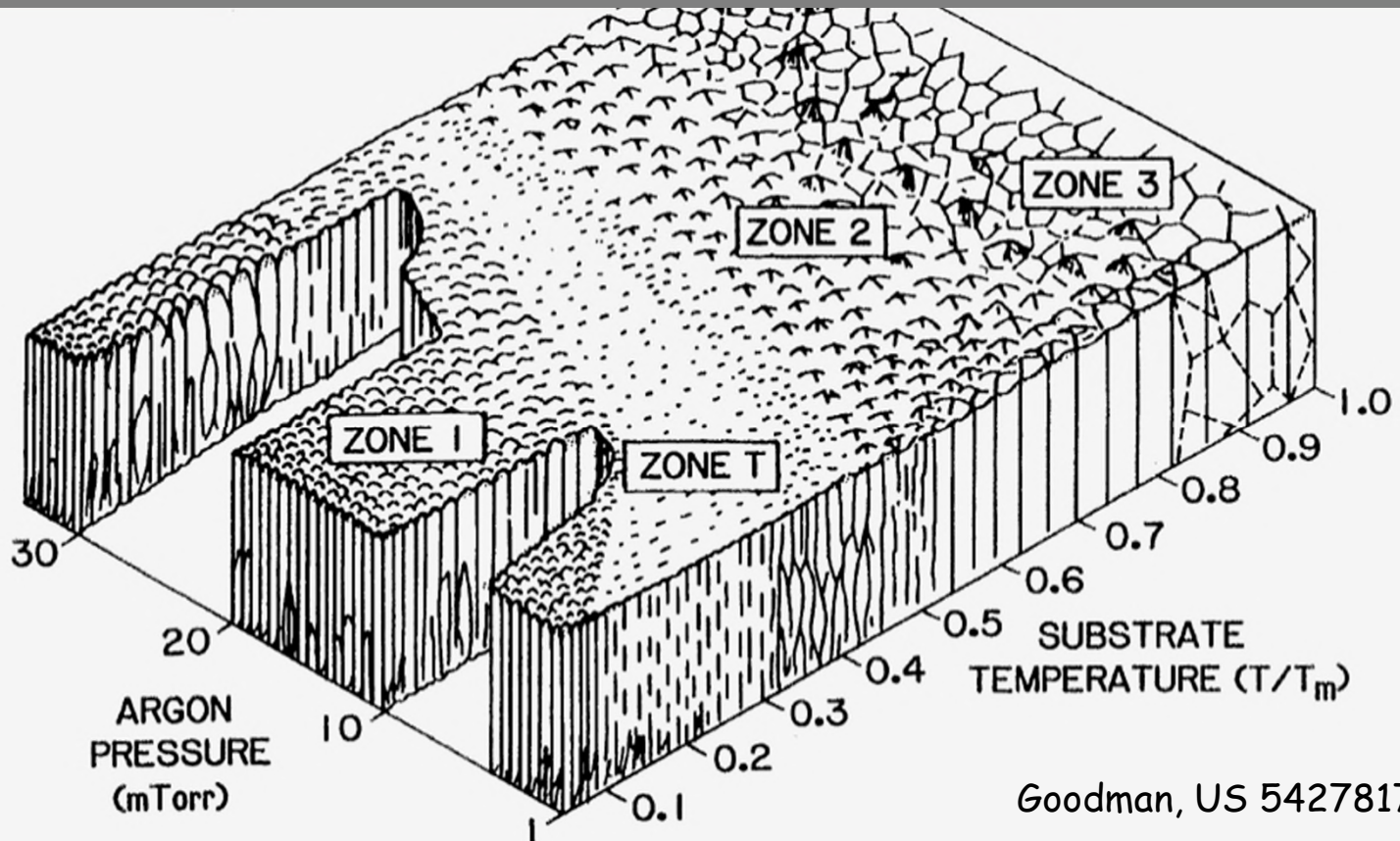


CsBr:Eu

Agfa Storage Phosphor

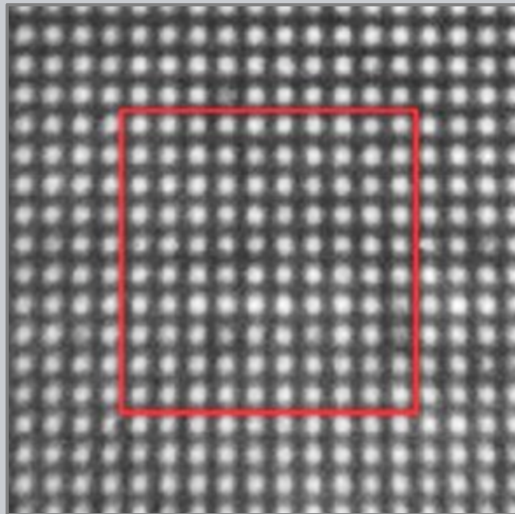
V.A.4.b - Scintillation material types

Needle morphology depends on the chamber pressure and substrate temperature during vapor deposition.



V.A.4.b - Scintillation material types

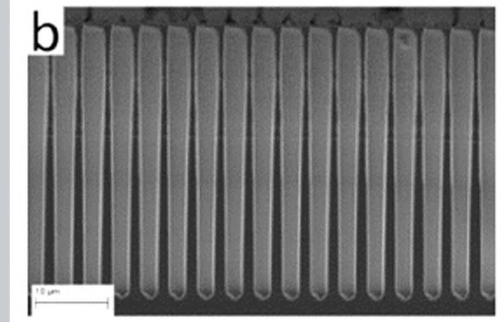
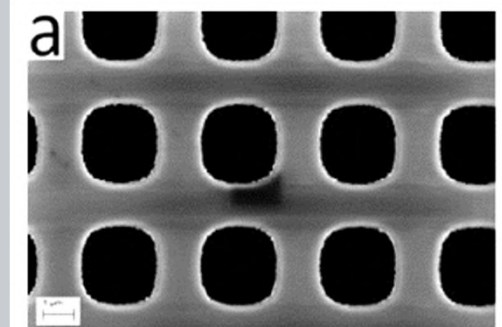
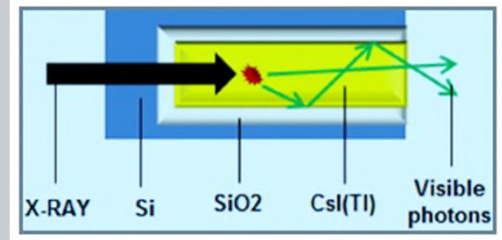
"Despite the simplicity of the [traditional] needle waveguiding concept, cross talk occurs between adjacent needles, since the structure lacks efficient optical isolation between the individual waveguides."



Minimal light dispersion is observed between pores

Structured CsI

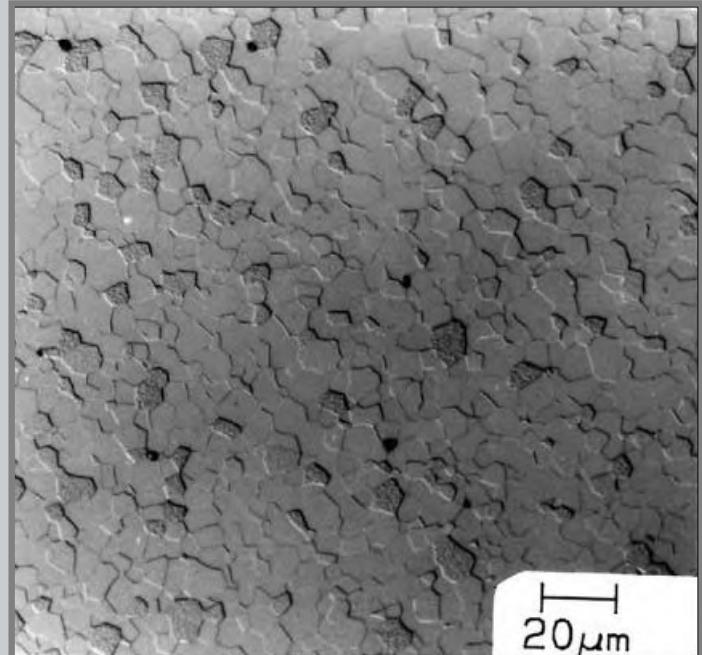
"...this problem was addressed by introducing a new type of detector which is based on a silicon pore array, filled with CsI(Tl)."



Hormozan Y, Sychugov I, and Linnros J (Sweden); High-resolution x-ray imaging using a structured scintillator, Med. Phys. 43 (2), February 2016.

Ceramic Phosphors

- Using a sintering process, compacted granular phosphors are transformed into transparent luminescent ceramics.
- The ceramic materials are uniformly doped with special additives that reduce afterglow.
- Ceramic scintillators have been used in x-ray CT scanners
 - $Y_{1.34}Gd_{0.60}Eu_{0.06}O_3$
 - $Gd_3Ga_5O_{12}:Cr,Ce$

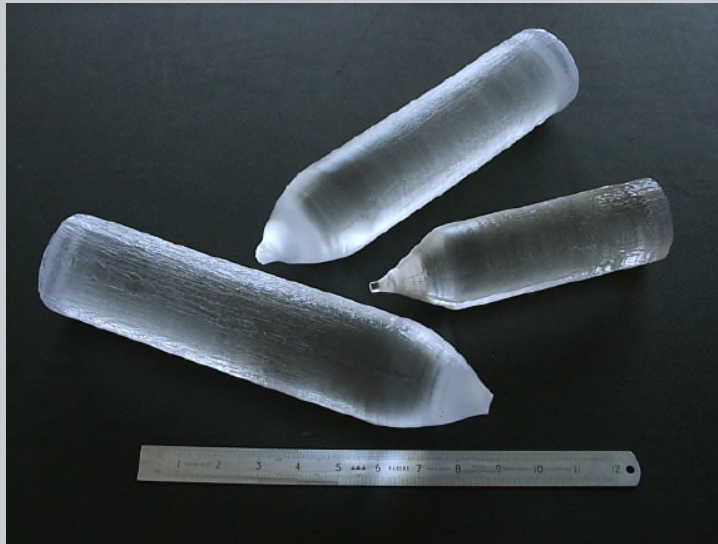


Microstructure of a polished and chemically etched section of a ceramic scintillator.

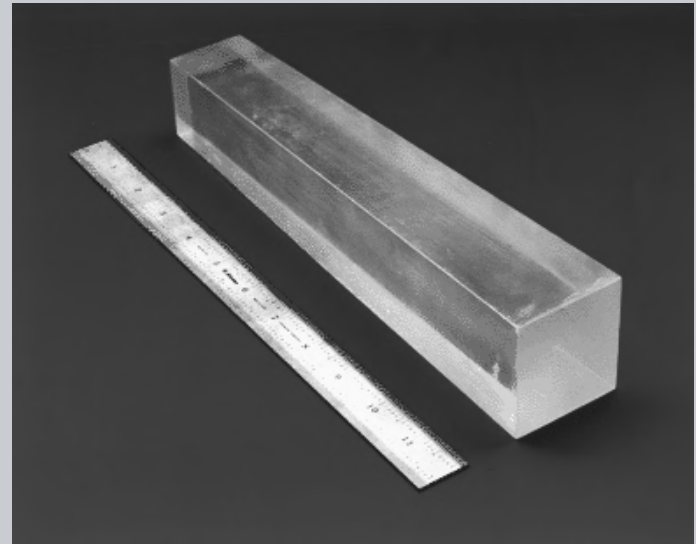
Greskovic 1997 Ann. Rev. Mater.
General Electric, CRD, NY

Solid crystals

- Solid crystals are grown out of a crystal 'seed' in the form of a 'boule'.
- Individual crystals are cut from the boule along crystal lattice surface to the size and shape desired.



LuYSiO (LYSO) Boule
Photonic Materials, CERN



CsI Crystal
Cornell

V.A.4.b - Scintillation material types

General Electric has recently developed a rare earth doped garnet scintillator with high light output and low afterglow.

These are now used in their computed tomography systems.



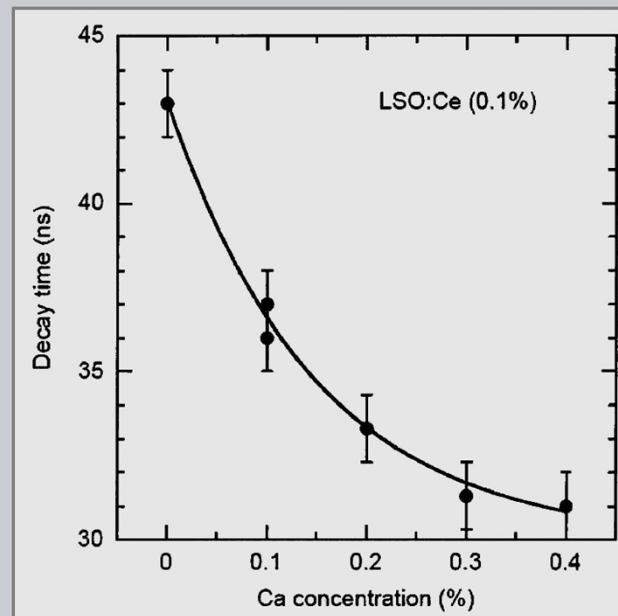
TABLE 1

From US patent 6630077 (2003)

Compostion	Light Output	Afterglow (%)	Speed (microseconds)	Stopping Power (1/cm at 70 keV)
$(\text{Tb}_{0.97}\text{Ce}_{0.03})_3\text{Al}_{4.9}\text{O}_{12}$	3	0.04	0.044	30.0
$(\text{Tb}_{0.72}\text{Lu}_{0.25}\text{Ce}_{0.03})_3\text{Al}_{4.9}\text{O}_{12}$	2	0.02	0.68	33.1
$(\text{Tb}_{0.47}\text{Lu}_{0.5}\text{Ce}_{0.03})_3\text{Al}_{4.9}\text{O}_{12}$	1.8	0.05	0.09	36.2
$(\text{Lu}_{0.97}\text{Ce}_{0.03})_3\text{Al}_5\text{O}_{12}$	1.6	1.84	0.06	42.6

V.A.4.b - Scintillation material types

Very fast decay time is important for PET systems that use time of flight analysis for reconstruction (Lecture 09). "LSO scintillation crystals with improved scintillation and optical properties are achieved by controlled co-doping a LSO crystal melt with amounts of cerium and an additional codopant such as calcium or other divalent cations." (US 8,278,624)



United States Patent US 8,278,624 B2 Oct. 2, 2012

LUTETIUM OXYORTHOSILICATE SCINTILLATION AND OPTICAL PROPERTIES AND METHOD OF MAKING THE SAME

Merry A. Koschan, Maryville, TN (US);
Charles L. Melcher, Oak Ridge, TN (US);
Piotr Szupryczynski, Knoxville, TN (U S);
A. Andrew Carey, Lenoir City, TN (U S)

Assignees:

Siemens Medical Solutions USA, Tennessee Research (US)



V.A.4.b - Scintillation material properties

From: van Eijk 2002, pg 89

	Density (g cm ⁻³)	ρZ^4_{eff} (10 ⁶)	Attenuation length at 511 keV (mm)/ prob. phot. eff. (%)	Hygro- scopicity	Light yield (photons/ MeV)	Decay time (ns)	Emission maximum (nm)
CsI:Na	4.51	38	22.9/21	Yes	40 000	630	420
CsI:Tl	4.51	38	22.9/21	Slightly	66 000	800→6 × 10 ³	550
CaWO ₄	6.1	89	13.6/32	No	20 000 ^b		420
YTaO ₄ :Nb	7.5	96	11.8/29	No	40 000 ^b		410
Gd ₂ O ₂ S:Tb	7.3	103	12.7/27	No	60 000 ^b	1 × 10 ⁶	545
Gd ₂ O ₂ S:Pr,Ce,F	7.3	103	12.7/27	No	35 000 ^b	4 × 10 ³	510
Gd ₂ O ₂ S:Pr (UFC)	7.3	103	12.7/27	No	50 000 ^b	3 × 10 ³	510
Y _{1.34} Gd _{0.60} O ₃ :(Eu,Pr) _{0.06} ^c (Hilight)	5.9	44	17.8/16	No	42 000 ^b	1 × 10 ⁶	610
Gd ₃ Ga ₅ O ₁₂ :Cr,Ce	7.1	58	14.8/18	No	40 000 ^b	140 × 10 ³	730
CdWO ₄	7.9	134	11.1/29	No	20 000 ^b	5 × 10 ³	495
Lu ₂ O ₃ :Eu,Tb	9.4	211	8.7/35	No	30 000 ^b	>10 ⁶	611



V.A.4.b - Scintillation material properties

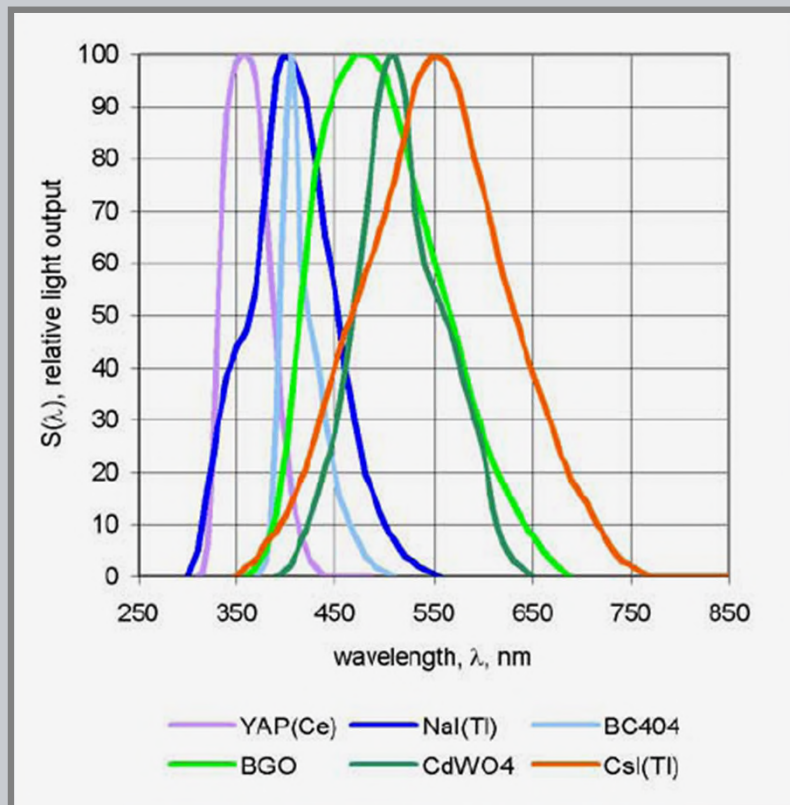
From: van Eijk 2002, pg 89

	Density (g cm ⁻³)	ρZ_{eff}^4 (10 ⁶)	Attenuation length at 511 keV (mm)/ prob. phot. eff. (%)	Hygro- scopicity	Light yield (photons/ MeV)	Decay time (ns)	Emission maximum (nm)
CaHfO ₃ :Ce	7.5	139	11.6/30	No	~10 000 ^b	40	390
SrHfO ₃ :Ce	7.7	122	11.5/28	No	~20 000 ^b	40	390
BaHfO ₃ :Ce	8.4	142	10.6/30	No	~10 000 ^b	25	400
NaI:Tl	3.67	24.5	29.1/17	Yes	41 000	230	410
LaCl ₃ :Ce	3.86	23.2	27.8/14	Yes	46 000	25 (65%)	330
LaBr ₃ :Ce	5.3	25.6	21.3/13	Yes	61 000	35 (90%)	358
Bi ₄ Ge ₃ O ₁₂ (BGO)	7.1	227	10.4/40	No	9 000	300	480
Lu ₂ SiO ₅ :Ce (LSO)	7.4	143	11.4/32	No	26 000	40	420
Gd ₂ SiO ₅ :Ce (GSO)	6.7	84	14.1/25	No	8 000	60	440
YAlO ₃ :Ce (YAP)	5.5	7	21.3/4.2	No	21 000	30	350
LuAlO ₃ :Ce (LuAP)	8.3	148	10.5/30	No	12 000	18	365
Lu ₂ Si ₂ O ₇ :Ce (LPS)	6.2	103	14.1/29	No	30 000	30	380



V.A.4.b - Scintillation emission spectrum

- Tabulated data on emission wavelength commonly lists the most probable wavelength.
- The emission is typically a broad distribution of wavelengths centered about the most probable.
- For some scintillations, the spectrum may contain a multitude of lines (not illustrated here).

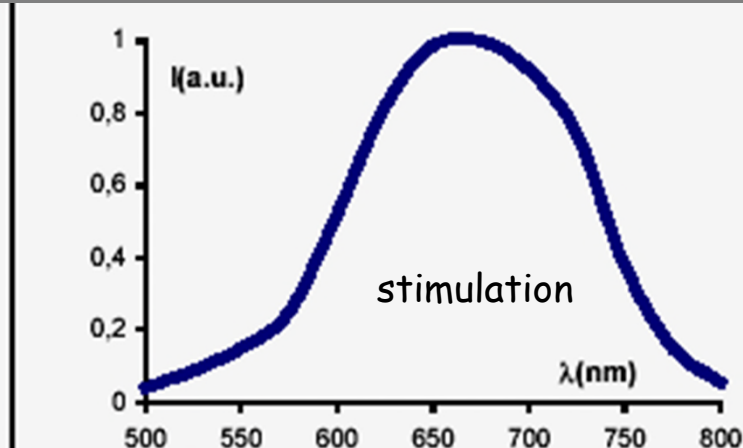
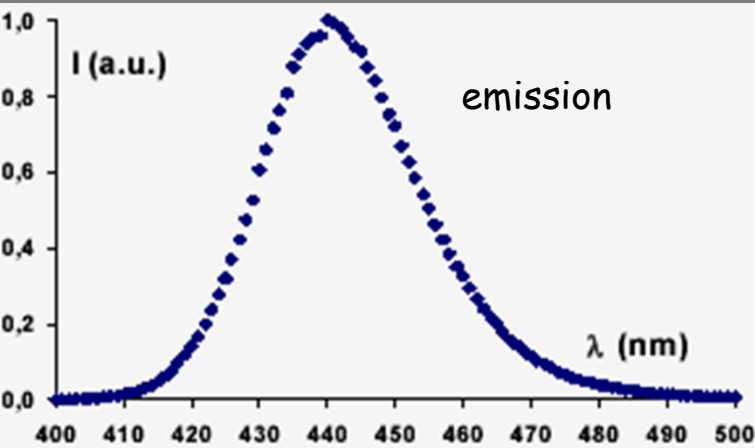


Electron Tubes Limited

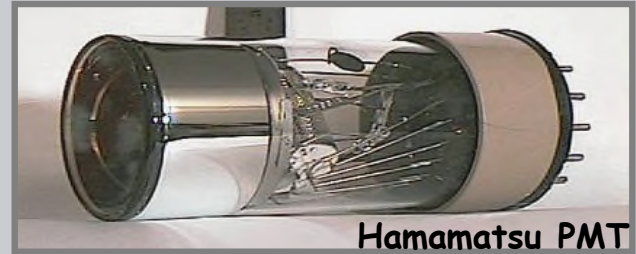
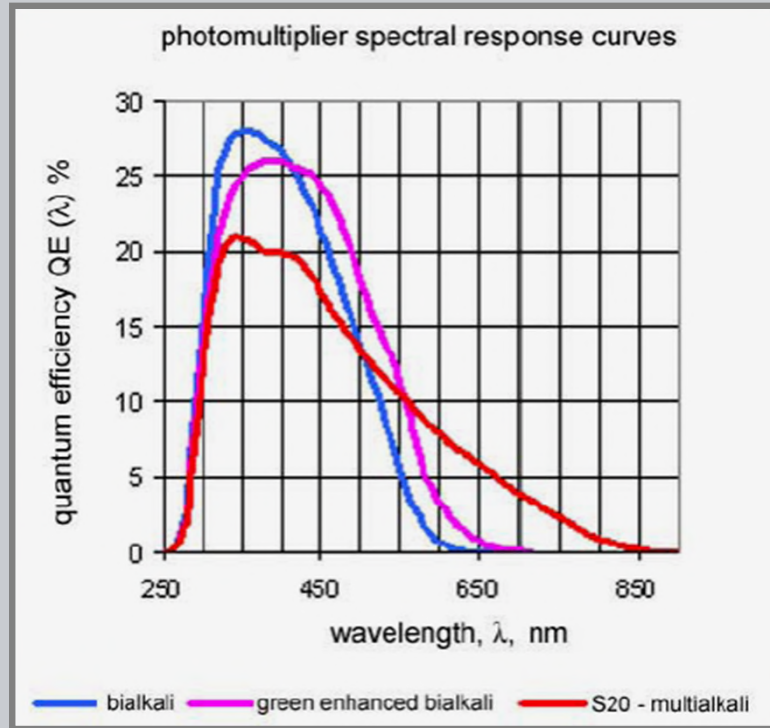
www.electrontubes.com

V.A.4.b - Stimulated emission spectrum

- For storage phosphors, the emission spectrum is typically in the blue region (~ 440 nm) that is well matched to PMT detectors.
- The stimulation spectrum is in the red region (~ 680 nm) that allows stimulation by laser beams from compact diode devices.



Emission and stimulation spectra of the Agfa CsBr:Eu storage phosphor material (Leblans, Agfa-Gevaert, Mortsel, Belgium)

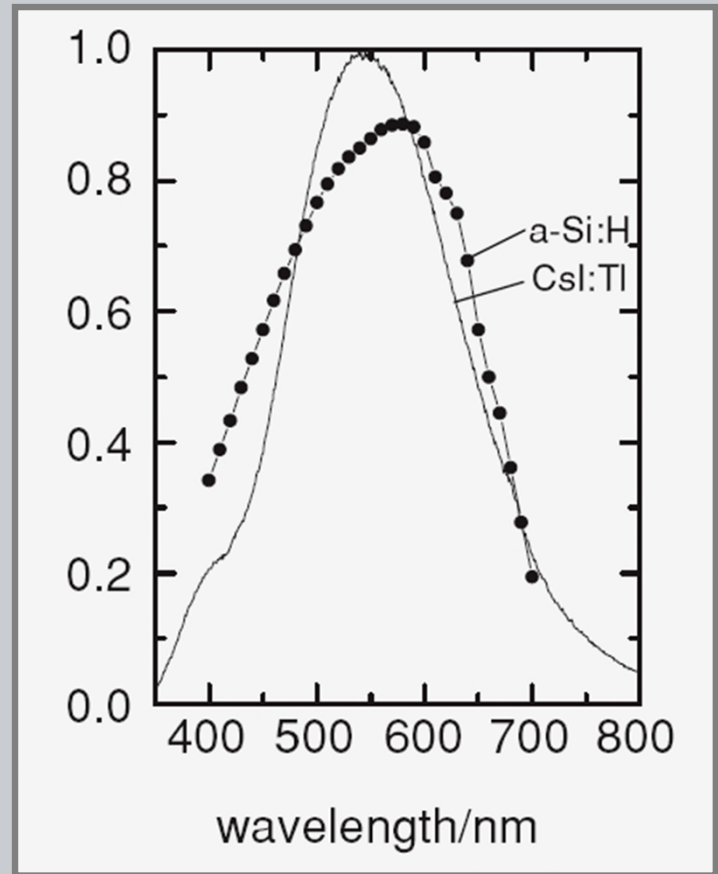


- Photomultiplier tubes (PMT) are often used to detect light in radioisotope imaging systems.
- The quantum efficiency of the light detection surface is best for blue light (350-450 nm).



Electron Tubes Limited
www.electrontubes.com

- Silicon photodiodes provide an alternative to PMTs for light detection.
- The quantum efficiency for most Si diodes is best for green and red light (500-650 nm). Advanced coatings can extend the response in the blue and/or infrared spectrum.
- Si CCD imaging detectors have similar spectral response.
- Arrays of Si diodes are used for flat panel radiography detectors with one diode for each detector element.



van Eijk 2002, figure 8
(Arbitrary Vertical Axis Units)

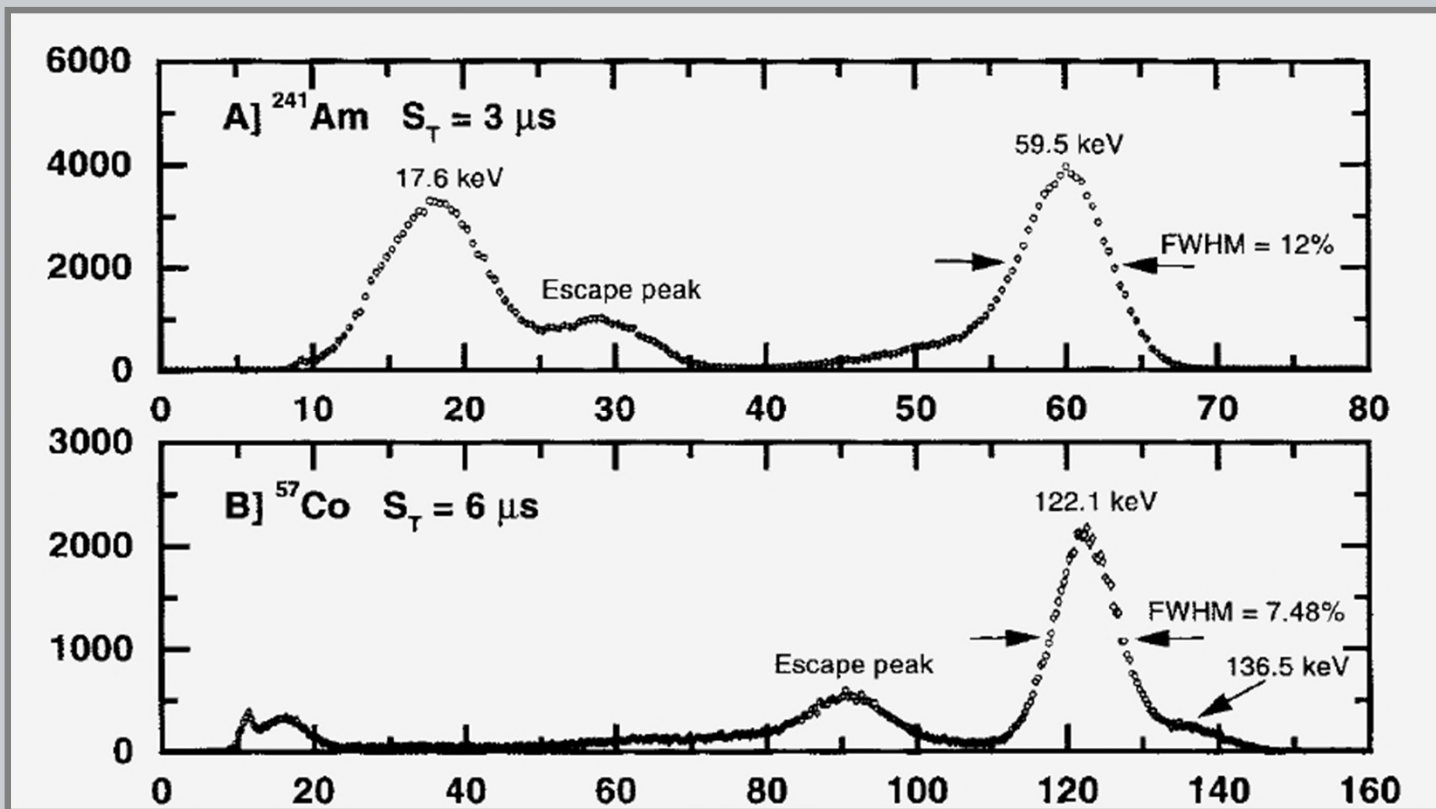


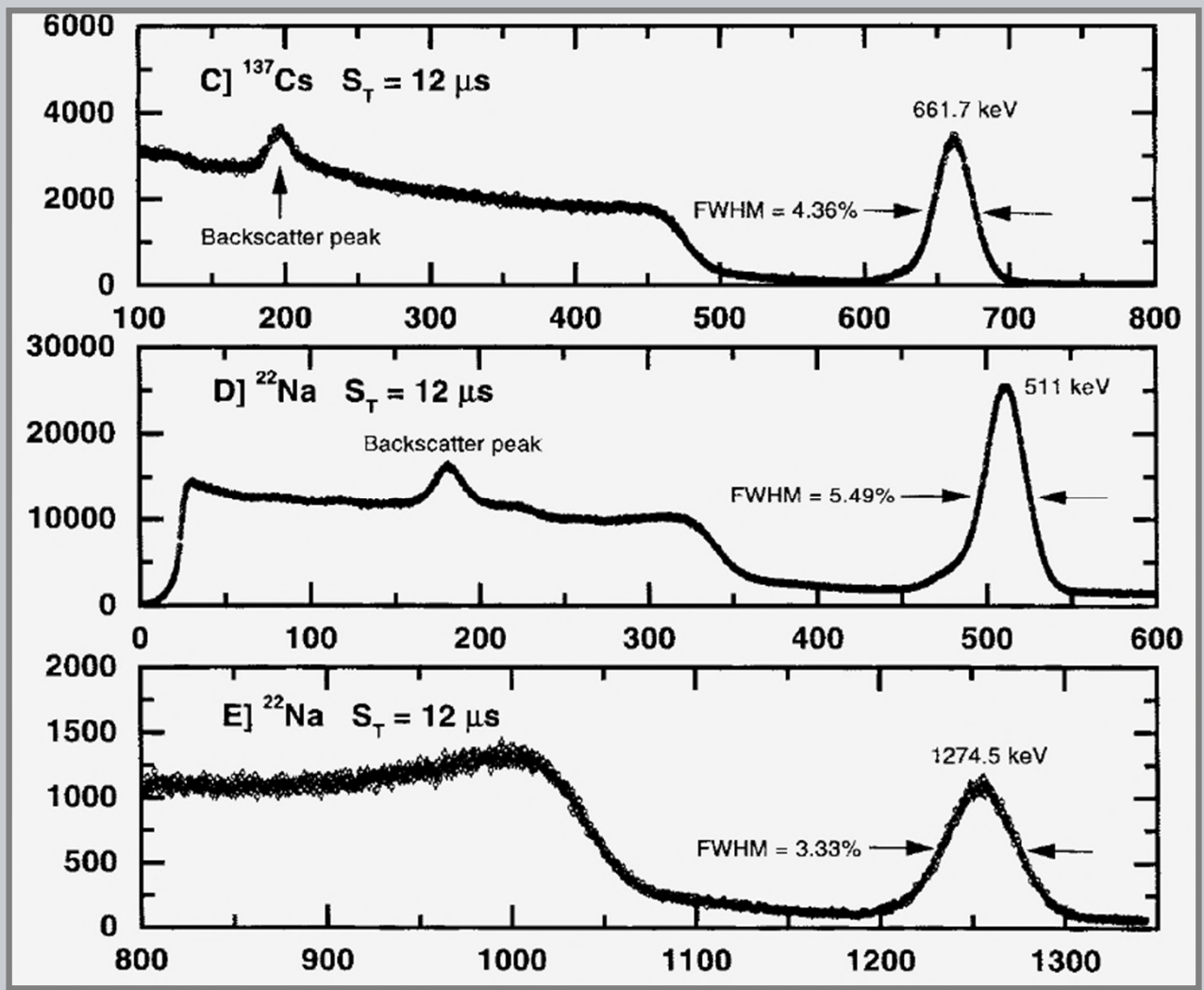
V.A.4.c - Indirect conversion efficiency

- Conversion of gamma energy to electrons.
 - photons/keV (NaI) 40
 - Light collection efficiency .50
 - Photo-conversion efficiency (PMT) .20
- Thus for 140 keV gamma rays (Tc 99m), we will collect 4 electrons/keV for a total of 560 electrons.
- The standard deviation in the signal associated with 560 electrons is 4.2% (i.e. $1/N^{\frac{1}{2}}$) which corresponds to a FWHM of about 9.7%.
- This is typical of the energy resolution of nuclear medicine Anger cameras using NaI crystals and PMT detectors.

V.A.4.d - Signal deposition probability (spectra)

Measured spectra from a CsI detector with a Si photodiode illustrate the improvement in the relative width of the full energy peak as the energy of the detected gamma ray is increased.

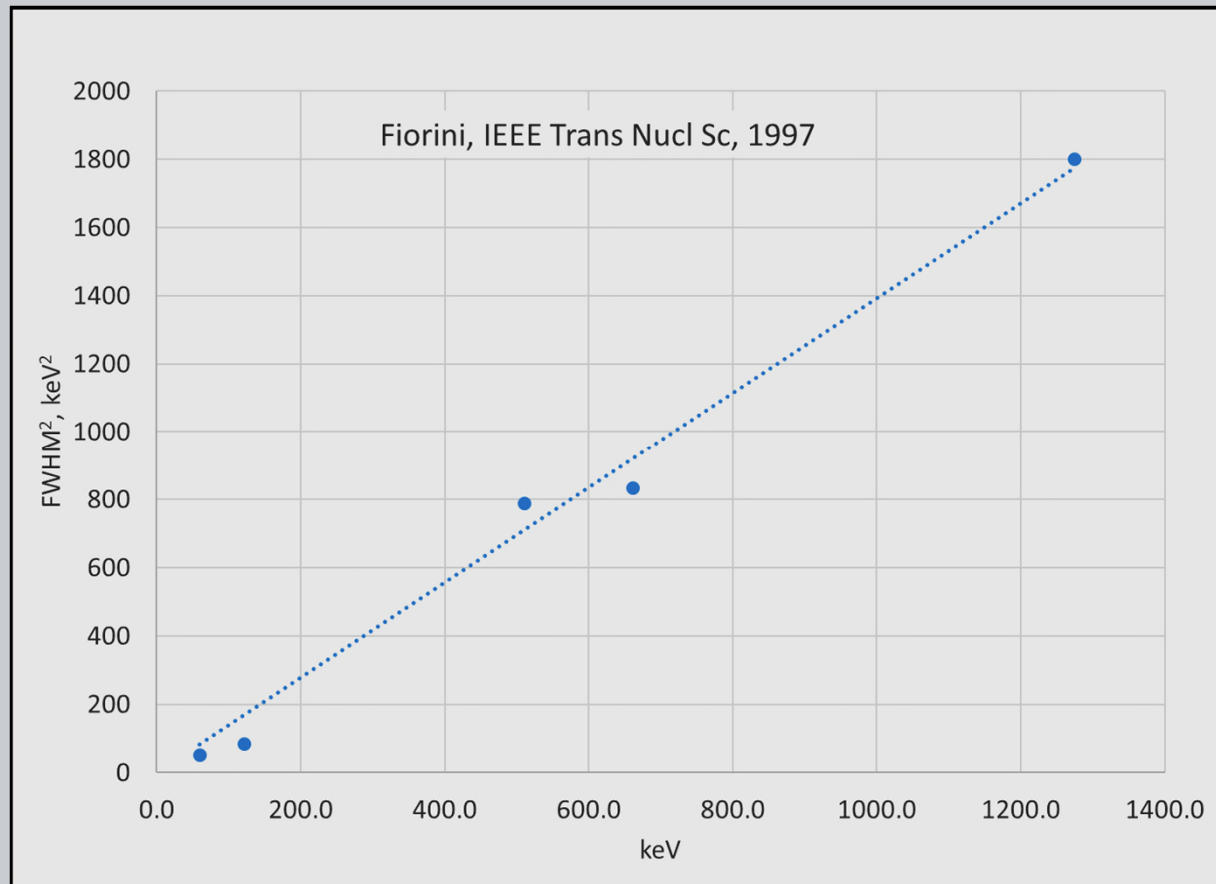






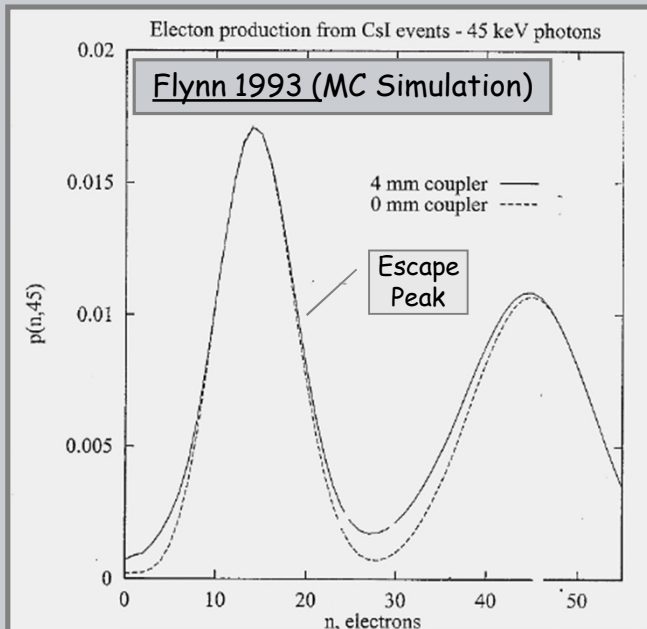
V.A.4.d - Signal deposition probability (spectra)

FWHM^2 should be proportional to the variance of the number of electrons and the deposited energy, E .



V.A.4.d - Signal deposition probability (spectra)

For thin screens used for x-ray imaging the escape probability for secondary radiation is high.



Simulations for the collected number of electrons agree with earlier experimental measures of the pulse height distribution.

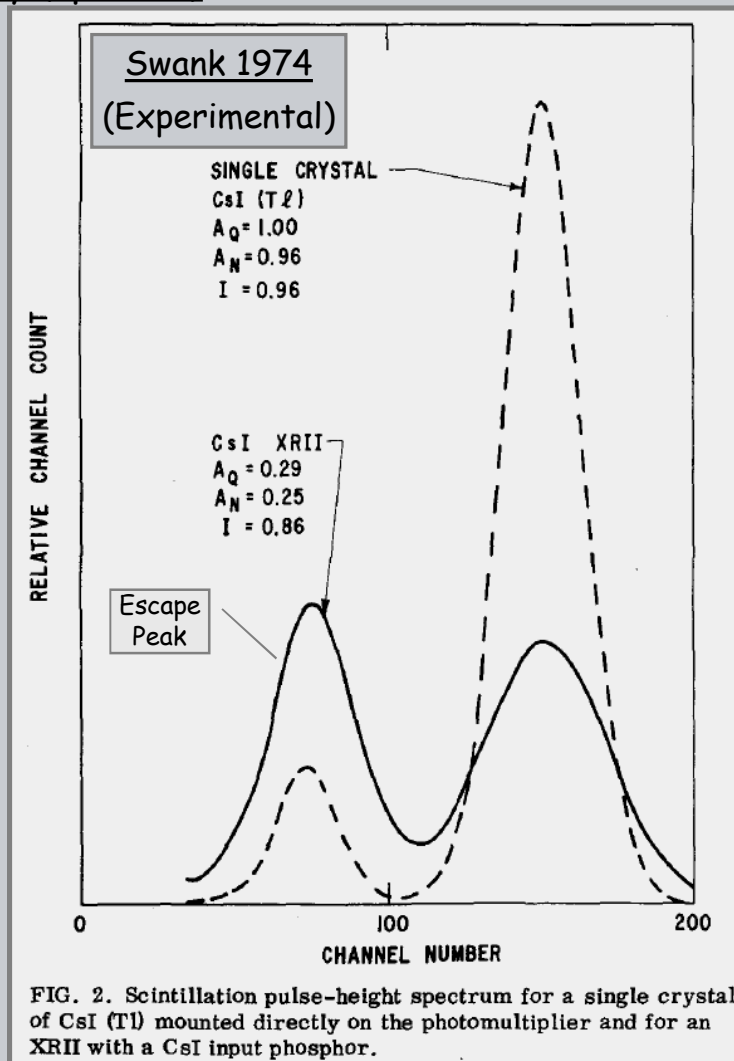


FIG. 2. Scintillation pulse-height spectrum for a single crystal of CsI (Tl) mounted directly on the photomultiplier and for an XR11 with a CsI input phosphor.



For granular screens, dispersion and absorption in the screen degrades the shape of the spectrum

